AEDC-TR-71-195

cy 2

EXTERNAL FLOW-FIELD EFFECTS ON THE PLUME IMPINGEMENT PRESSURE AND HEAT-TRANSFER-RATE DISTRIBUTIONS ON A FLAT PLATE

W. T. Strike, Jr. and D. E. Boylan

ARO, Inc.

September 1971

VON KÁRMÁN GAS DYNAMICS FACILITY
ARNOLD ENGINEERING DEVELOPMENT CENTER
AIR FORCE SYSTEMS COMMAND
ARNOLD AIR FORCE STATION, TENNESSEE

NOTICES

When U. S. Government drawings specifications, or other data are used for any purpose other than a definitely related Government procurement operation, the Government thereby incurs no responsibility nor any obligation whatsoever, and the fact that the Government may have formulated, furnished, or in any way supplied the said drawings, specifications, or other data, is not to be regarded by implication or otherwise, or in any manner licensing the holder or any other person or corporation, or conveying any rights or permission to manufacture, use, or sell any patented invention that may in any way be related thereto.

Qualified users may obtain copies of this report from the Defense Documentation Center.

References to named commercial products in this report are not to be considered in any sense as an endorsement of the product by the United States Air Force or the Government.

EXTERNAL FLOW-FIELD EFFECTS ON THE PLUME IMPINGEMENT PRESSURE AND HEAT-TRANSFER-RATE DISTRIBUTIONS ON A FLAT PLATE

W. T. Strike, Jr. and D. E. Boylan
ARO, Inc.

FOREWORD

This report summarizes work sponsored by the Arnold Engineering Development Center (AEDC), Air Force Systems Command (AFSC), Arnold Air Force Station, Tennessee, under Program Element 65802F.

The results were obtained by ARO, Inc. (a subsidiary of Sverdrup & Parcel and Associates, Inc.), contract operator of the AEDC under Contract F40600-72-C-0003. This report contains experimental data obtained during the period from March 9 to 16, 1971, under ARO Project No. VT2128, and the manuscript was submitted for publication on July 14, 1971.

This investigation was proposed by Mr. C. J. Schueler, Chief of the Aerodynamics Division of the von Kármán Gas Dynamics Facility (VKF). Also, the authors are indebted to Mr. L. Ray Baker of the Lockheed Missiles and Space Company, Huntsville Research and Engineering Center, for the theoretical results which are included in this report.

This technical report has been reviewed and is approved.

Emmett A. Niblack, Jr.
Lt Colonel, USAF
AF Representative, VKF
Directorate of Test

Joseph R. Henry
Colonel, USAF
Director of Test

ABSTRACT

Experimental plume impingement pressure and heat-transfer-rate distributions on a flat plate with and without an external Mach number 18 stream are described. The plume was generated by expanding helium through a 1.61 area ratio nozzle, which simulated the initial shape of a rocket exhaust plume produced by a nozzle with an area ratio of 25 operating at an altitude of 262,000 ft. Although the plume generator nozzle conditions were not varied, the quiescent environment conditions and external stream conditions were adjusted so that the general shape and size of the plume remained the same. A higher quiescent pressure environment was required to produce a plume of the same size as the plume obtained in an external stream. In the immediate vicinity of the plume impingement on the flat plate within the plume boundary, the pressure distributions obtained with and without external flow were identical, but the overall change in surface loading produced by the plume was significantly affected by the external stream. The external stream also caused the local heat-transfer rates to increase significantly in the immediate vicinity of the plume boundary impingement point on the flat plate. Therefore, any general assumption that aerodynamic external flow-field effects on plumes and on plume impingement loading and heat-transfer rates is negligible, even at an altitude of 262,000 ft, should be carefully examined.

CONTENTS

APPENDIXES

I. ILLUSTRATIONS

Figure

NOMENCLATURE

A	Plume generator nozzle exit area, $(\pi/4)d_e^2$, in.^{2}
A*	Plume generator nozzle throat area, in.^{2}

C_p	Specific heat at constant pressure, Btu/lbm - °K
d_e	Plume generator nozzle exit diameter, in.
f_N	Centerline plume impingement loading factor, see Table VI
h_o	Stagnation enthalpy, Btu/lbm
L	Flat plate length, in.
M	Mach number
$\dot{m}$	Flow rate, lbm/sec
p	Static pressure, psia
p_o	Stagnation pressure, psia
p_o'	Total pressure downstream of a normal shock, psia
q_∞	Free-stream dynamic pressure, psia
$\dot{q}$	Heat-transfer rate, Btu/(ft^2-sec)
Re/in.	Reynolds number, per inch
Re_ℓ	Reynolds number based on the length, L
St_j	Stanton number reference to the helium plume properties, $\dot{q}/[\dot{m}_j\ (h_{o_j} - C_{p_j}\ T_w)]$
T	Static temperature, °K
T_o	Stagnation temperature, °K
u_∞	Free-stream velocity, ft/sec
X_m	Displacement of the flat plate leading edge relative to the plume generator nozzle exit, $X_m = x - x'$, in.
x,y,z	Coordinates referenced to the center of the plume nozzle exit plane, in.
x',y',z'	Coordinates referenced to the flat plate leading edge, in.
γ	Ratio of specific heats

λ_∞ Free-stream mean-free-path length, in.

ρ Density

SUBSCRIPTS

b Chamber property without external flow

j Plume generator nozzle exit property

w Flat plate wall value

∞ Free-stream or external stream property

SECTION I
INTRODUCTION

One of the problems associated with the abort and normal staging maneuvers of the orbiter and booster vehicles of the Space Transportation System (STS) concerns the plume impingement pressure and thermal loadings imposed on the vehicles as they separate. Even under normal conditions, the orbiter engines may be ignited before the vehicles separate; and, during the separation maneuver, the rocket exhaust of the orbiter may impinge upon the surface of the booster. Therefore, the analytical techniques (for example, see Ref. 1) and ground testing simulations employed to evaluate this plume impingement problem must be carefully examined.

A Captive Trajectory System (CTS) is being designed and fabricated by the von Kármán Gas Dynamics Facility (VKF), AEDC, for use in the continuous Wind Tunnels A/B and C. One proposed use of this CTS system will be to evaluate the aerodynamic staging characteristics of the Space Transportation System configurations. Therefore, one purpose of this investigation was to determine whether or not an auxiliary gas supply system should be included in the CTS system to simulate aerodynamic plume effects.

It seems reasonable to expect that at extremely high altitudes (200,000 ft or more), most of the loading generated can be attributed to the rocket exhaust plume impingement. This suggests that the plume impingement can be evaluated in the absence of an external stream if the plume size and momentum distribution are properly simulated. Some attempt must be made however, to determine the altitude at which external flow-field effects on the plume size and shape are negligible or, more precisely, the altitude above which the plume impingement loading is not affected by an external stream.

Therefore, the second purpose of this test was to examine some of the loading characteristics generated on a flat surface by a plume in the presence and absence of an external stream. Without external flow, the plume expanded into a quiescent environment with a pressure of 310 to 395 μHg, whereas with external flow (a Mach number 18.2 stream), the plume expanded into a flow field with a static pressure of 6 μHg. The plume was produced by exhausting helium through a nozzle with an area ratio of 1.61 into the Low Density Hypersonic Wind Tunnel (M) of the von Kármán Gas Dynamics Facility. A flat plate was supported in close proximity to the plume generator (within 1.25 to 5.0 plume nozzle exit diameters). Test data in the form of flat plate heat-transfer-rate and pressure measurements were obtained with and without the free-stream flow.

SECTION II
TEST EQUIPMENT AND PROCEDURES

2.1 WIND TUNNEL

Tunnel M, shown schematically in Fig. 1, is a continuous, arc-heated, low density, free jet, hypersonic wind tunnel normally using nitrogen as the test gas. A rotating-arc-type d-c arc heater of VKF design with a 200-kw power supply is used to raise the tunnel

gas reservoir temperature to about 2900°K at a pressure of approximately 19 atm. The gas expands through an axisymmetric, aerodynamically contoured nozzle with an 0.181-in. throat diameter and a 35.1-in. exit diameter. The flow leaves the nozzle as a free jet exhausting into an 8-ft-diam test chamber containing a diffuser consisting of a convergent inlet, a constant area throat section, and a divergent outlet. The resulting test core of uniform flow is 6 to 10 in. in diameter and about 50 in. long with a nominal Mach number of 18.2 and unit Reynolds number of 1250 per inch. The pumping required to operate this test unit is provided by three stages of air ejectors which are located in series and exhaust into the VKF main compressor system through the VKF Tunnel C test section.

2.2 MODEL

The model (Fig. 2) was a copper plate (7.5 by 11.5 in.) with a brass sharp leading edge. The model leading edge and flat plate surface containing the instrumentation were water cooled by means of the cooling lines. This cooling system maintained the model wall temperature at 315°K during the test.

The relative size and nominal location of the pressure taps and the heat-transfer gages are shown schematically in Fig. 2a. The solid symbols locate the pressure taps, and the larger open circles represent the heat gage locations. A view of the compartment containing the instrumentation leads and the water cooling lines in the flat plate is shown in Fig. 2b, which is a photograph of the lower surface of the flat plate.

A schematic of the plume generator is shown in Fig. 3a. This is a cone-cylinder boat-tailed body with a low area ratio nozzle located in the base. The plume generator support consisted of two cylindrical tubes, one of which was used to supply heated helium gas to the body. The other tube was connected to the transducer for measuring the chamber pressure and contained the thermocouple leads for measurement of the gas temperature. The area ratio of the nozzle was 1.61 with a nominal exit angle of 10 deg and an 0.314-in.-diam nozzle throat.

The orientation of the plume generator relative to the flat plate, and the associated coordinate system for this test installation, is shown in Fig. 3b. An electric drive system was used to remotely position the flat plate leading edge relative to the plume generator exit, that is, X_m was varied with the tunnel running. The variation in displacement of the flat plate surface from the plume generator axis (variation in y) was accomplished by moving the flat plate and reattaching the vertical model support in a new position with the tunnel off.

A schematic and a photograph of the test installation are shown in Fig. 4. This figure also summarizes the type of measurements made during this test program. As shown in Fig. 4b, the original size of the plate was 10 by 11.5 in., but because of tunnel blockage problems, the plate span was reduced by 2.5 in.

2.3 PLUME GENERATOR GAS SUPPLY

Helium gas was selected to generate the plume because it has a very low condensation temperature. The gas originated from a 2000-psia source and was heated initially by passing the gas through two parallel-connected, single-pass, hot core, Kanthal® element resistance heaters. The tunnel flow (total temperature of 2900°K) impinging on the gas supply line supporting the plume generator provided an additional heat input which elevated the helium plume gas temperature to about 680°K. The total pressure of the gas in the plume generator reservoir was maintained at 5.50 psia during the test program. At these test conditions, the helium plume simulated the plume produced by a nozzle with an exit area ratio of 25, a chamber pressure of 440 psia, and using a gas with a ratio of specific heat of 1.27 at an altitude of 262,000 ft (see Ref 2).

2.4 INSTRUMENTATION AND ESTIMATED REPEATABILITY

The Tunnel M instrumentation used to determine tunnel flow conditions consists of power supply control monitors and stilling chamber pressure measurements, which are used to determine the tunnel mass flow rates, and an impact pressure probe located at the tunnel nozzle exit. As indicated in Fig. 4a, the model measurements consisted of monitors to record model position, a model pressure measuring system using 3- and 30-mm Hg MKS Baratron® pressure meters, and high sensitivity steady-state heat-transfer gages.

Tunnel stilling chamber conditions are determined by a direct reading of the reservoir pressure and the pressure upstream of the sonic or mass flow orifices, with 500- and 1500-psid transducers, respectively. These tunnel reservoir measurements, along with the impact pressure measurement at the tunnel nozzle exit and equilibrium thermodynamic properties of the gas, were used to define the free-stream conditions. The tunnel mass flow rate, the reservoir pressure, the sonic orifice discharge coefficient, and the real gas thermodynamic properties for nitrogen are used to deduce the stilling chamber bulk temperature. The estimated repeatability of the free-stream flow field properties are given in Table I (Appendix II).

The model pressure measuring system consists of three high sensitivity transducers mounted within the tunnel test cell. The pressure ranges varied from 10 μHg to 30 mm Hg, depending on transducer sensitivity. Each transducer was individually calibrated during each operating shift using a U-tube oil manometer with a resolution of ±1.5 μHg.

The model heat-transfer rates were recorded by high sensitivity transducers which were developed in the VKF and derive their basic principle of operation from the Gardon gage (Ref. 3), but have a sensitivity to incident heat flux which is more than an order of magnitude higher. The nominal dimensions of these heat flux units are 0.25-in. O.D. by 0.38 in. and because of material considerations are limited to a maximum service temperature of less than 450°K.

Experimental calibration of the high sensitivity transducer is accomplished with a radiant heat source. Calibration is achieved by exposing one or more test transducers to the same incident heat flux and measuring the output from each simultaneously. This

procedure is repeated at different heat flux levels. Heat flux measurement standards are slug calorimeters which are designed and manufactured at the VKF. All VKF transducer calibrations are traceable to slug calorimeter standards. Heat-transfer standards used with the radiant heat flux calibration facility are conventional Gardon-type transducers. In addition to calibration against slug calorimeter standards, calibration checks were also performed on three heat-transfer, standard Gardon-type transducers at two independent calibration facilities. Calibration agreement was within four percent for the three heat-transfer standards checked. The good agreement of VKF calibrations with those performed at two other calibration facilities enhanced the credibility of VKF heat flux calibration techniques and standards. Absolute accuracy of heat flux calibrations is believed to be within ±5 percent, and repeatability and linearity are ±3 percent.

The flat plate position was adjusted by a mechanism which has two degrees of freedom, providing a remotely controlled rotational and translational motion. With the translational motion and a manual adjustment of the arm length of the rotational component (see Fig. 4a), the model could be positioned within ±0.01 in. in the axial position and ±0.05 in. in the Y or radial arm position.

The plume generator plenum pressure was measured with a 5-psid transducer and the temperature with a Chromel®-Alumel® thermocouple.

These temperature, pressure, and heat-transfer measuring systems result in uncertainty or repeatability in the flat plate test parameters as deduced in some cases from a Taylor series method of error propagation (Table II).

SECTION III
TEST CONDITIONS

In the absence of an external stream. the helium plume expanded into a nearly quiescent environment in Tunnel M in which the pressure generally varied from 315 to 395 μHg. The external flow condition was produced by expanding arc-heated nitrogen gas through the Tunnel M contour nozzle to produce a Mach number 18.2 stream with a static pressure of 6 μHg. The Mach number 18.2 external stream flow properties are listed in Table III. The corresponding helium plume generator conditions are listed in Table IV. The internal properties and boundary characteristics of the helium plume expanding into the Tunnel M Mach number 18 external stream in the absence of the flat plate were evaluated experimentally and reported in Ref. 3 by Norman, Kinslow, and Lewis.

The flat plate plume impingement pressure and heat-transfer-rate data were obtained with the model leading edge located at various positions from 5 in. upstream to 10 in. downstream of the plume generator exit plane. The flat plate was moved parallel to the plume generator axis at vertical displacements (y/d_e) of 1.25, 2.5, 3.75, and 5.0 from the plume axis. At the y/d_e locations of 1.25 and 5.0, plume impingement data were obtained only for the quiescent condition. One set of data was obtained with the flat plate at y/d_e of 2.5, with the external flow on and the plume generator off. A test summary is given in Table V.

SECTION IV
RESULTS AND DISCUSSION

Initially, a set of flat plate pressure and heat-transfer-rate distributions was obtained with the external stream on and the plume generator off. These data were obtained to define the effects of the wake produced by the cone-cylinder plume generator on the flat plate distributions. The results obtained with the flat plate at $y/d_e = 2.5$ and $X_m = 0$ are shown in Fig. 5. Although the plume is not present, the plume properties such as the nozzle chamber pressure (p_{o_j}) and the plume mass flow and stagnation enthalpy were used to normalize the pressure and heat-transfer-rate data in order to simplify comparisons with data taken with the plume on.

An estimate of the heat-transfer-rate and pressure distributions on a flat plate with a sharp leading edge in an undisturbed hypersonic stream based on the analytical results of Rudman and Rubin (Ref. 4) is included in Fig. 5. In comparison to these theoretical results and some previously unpublished flat plate data obtained in the undisturbed flow of Tunnel M, the present data indicate that the plume generator wake increased the heat-transfer rates by a factor of 5.2 to 6.3, and increased the pressure loading by a factor of 1.3 to 2.0.

The theoretical locations of the plume boundary with and without external flow shown in Fig. 6 were obtained from the method-of-characteristics plume computer program of Lockheed Space and Missile Company (Ref. 5). These computations were made using the experimental test conditions as program inputs. The results indicate that the general size and initial shape of the plume are similar for the cases of a plume expanding into a quiescent environment with a plume boundary pressure of 4.63×10^{-3} psia (240 μHg) and into a hypersonic stream at a Mach number of 18 and a free-stream static pressure of 1.2×10^{-4} psia (6.2 μHg). The range of positions of the flat plate in the plume during this test is also shown. As the flat plate is displaced further from the plume axis (increase in the y coordinate), the plume boundary impingement point on the plate becomes a more sensitive function of the plume boundary shape. Thus, small differences in plume boundary shape can have significant effects on the plume impingement loading distribution.

Figure 7 gives the flat plate pressure distribution along the ray of taps located in the vertical plane of symmetry of the plume, which was always perpendicular to the flat plate surface. The measured flat plate wall pressures (p_w) are normalized by the plume generator chamber pressure (p_{o_j}). The distributions with no external flow and the plate located 2.5 and 3.75 nozzle exit diameters above the plume axis are given in Figs. 7a and b. Figures 7c and d give the corresponding results with the external free-stream flow.

The flat plate instrumentation was limited by the small number of channels that can be recorded in Tunnel M; consequently the pressure and heat-transfer-rate distributions presented were obtained by recording all instrumentation outputs with the plate leading edge at various axial locations relative to the exit plane of the plume generator nozzle for fixed y/d_e positions. The assumption was made and somewhat borne out by these results that the plume impingement loading is primarily a function of the distance from the plume generator nozzle exit. Thus, it was expected that the location of the flat plate

leading edge in the flow field would have a negligible effect on the resulting plume induced impingement flow field.

As indicated in Figs. 7a and b, in the absence of an external stream, there is a small but measurable effect on the flat plate pressure and heat-transfer-rate distributions produced by varying the location of the plate leading edge. With the plate leading edge forward of the plume boundary (i.e., according to Fig. 6, $X_m < 2$ in. at $y/d_e = 2.5$ and $X_m < 4$ in. at $y/d_e = 3.75$), the flow along the flat plate overexpands and then recompresses to the quiescent pressure. With the leading edge downstream or aft of the plume boundary (solid symbols), the pressure distribution shows an additional pressure peak before the pressure decays to the quiescent value.

Apparently, for this quiescent condition, the Mach disc usually present in an underexpanded plume is located close to the aft section of the flat plate. When the leading edge is located within the plume boundary, the Mach disc moves upstream toward the plume generator nozzle. Obviously, the presence of the flat plate in the plume will alter the expanding flow field of the plume, and this will cause the Mach disc to move upstream. The presence of the plume Mach disc on the flat plate would cause the additional pressure peak (solid symbols) noted in Figs. 7a and b.

The effect of the Mach disc location on the impingement pressure loading could be eliminated by decreasing the pressure of the quiescent environment which would move the Mach disc downstream of the flat plate. However, a reduction in the plume boundary pressure would produce a larger plume and alter the plume impingement loading. Once the leading edge of the plate is within the plume boundary, the plume impingement loading becomes a function of the flat plate location in the plume (i.e., $p_w = f(X_m)$ when $X_m > 1.3$ at $y/d_e = 2.5$ and $X_m > 2.4$ at $y/d_e = 3.75$).

In an external stream as shown in Figs. 7c and d, the variation in the model leading edge location did not affect the plume impingement pressure loading on the flat plate when plotted as a function of the distance aft of the nozzle exit plane. Eventually, the plume boundary pressure approaches the external stream static pressure which in the present test was nearly two orders of magnitude smaller than the back pressure needed to produce the same size plume in a quiescent environment.

The theoretical estimates of the plume impingement pressure loading (solid curves in Figs. 7a and b) were obtained by using the theoretical inviscid method-of-characteristics solutions of the helium plume flow field (Ref. 1). This solution provides values for the local Mach number, flow direction, and static pressure in the plume flow field. The local impact pressure was obtained by using the oblique shock relationships which relate the approaching stream Mach number and flow deflection angle to the static pressure rise through an oblique shock wave. The flow deflection angle was defined as the angle between the plate and the local impinging plume flow field direction.

Thus, the pressure law used corresponds to the tangent wedge approximation. In part, the purpose of these tests was to determine the applicability of this law to the nonuniform flow fields present in a plume. An examination of Fig. 7 shows that the

agreement between theory and experiment is satisfactory for a region aft of the maximum pressure peak. Forward or upstream of this peak, the experimental pressure distributions are more rounded, whereas further downstream of the peak the distributions obtained in the absence of an external stream are affected by the Mach disc location in the plume, as discussed earlier, which is not accounted for in this theory.

In the case of an external stream, the theoretical analysis of the plume flow field assumes that the pressure along the plume boundary varies in a manner prescribed by the Newtonian impact theory. The external stream pressure based on the free-stream Mach number, ratio of specific heats, static pressure, and local slope of the plume boundary is matched to the internal plume boundary pressure as evaluated by the plume flow field method-of-characteristics solution. As shown in Figs. 7c and d, in this case the theory does not provide a very good estimate of the plume boundary impingement point and also underestimates the region of plume impingement loading for these conditions.

The discontinuity in the theoretical pressure distribution, that is, the decrease in pressure as one moves rearward of the peak pressure, is due to an internal shock within the plume. This discontinuity was not observed in any of the present experimental distributions. Also, intuition suggests that in the presence of an external stream there should be a pressure peak immediately upstream of the plume impingement point, indicating the presence of a plume bow wave impinging on the flat plate. There is a smaller pressure peak at x = -1.0 in. in Fig. 7c, but this peak corresponds more closely to the point where the plume generator bow wave would theoretically impinge on the flat plate. Probably, the mixing region of the plume boundary has smeared out not only the internal plume compression wave but also the external stream plume bow wave.

As expected, the discrepancy between the theory and the experimental results increases as the plate is displaced further from the plume axis, as may be seen in comparing Figs. 7c and d. The sensitivity of the actual location of the impingement point on the plate is a stronger function of the plume shape as the plate is displaced further from the plume axis. In fact, a slight change in the plume boundary conditions will alter the plume impingement point and possibly the plume impingement pressure distributions; for example, note that the repeatability of the distributions at y/d_e of 3.75 is poorer than those obtained at a y/d_e of 2.50. In this case, the repeatability of the distributions is related to the repeatability of establishing the same nozzle chamber to external plume boundary properties such as p_{o_j}/q_∞ or p_{o_j}/p_b.

In the region of the peak pressure point, the experimental distributions obtained with and without external flow match as shown in Fig. 8a which compares the data from Figs. 7a and c. A similar, but poorer, comparison exists for the distributions obtained at y/d_e of 3.75 (Fig. 8b). This suggests that the plume size and shape are in better agreement than indicated by the theoretical estimates of the plume boundary locations shown previously in Fig. 6.

Although the pressure distributions in the immediate vicinity of the peak pressure point were not affected by the presence of an external stream (Fig. 8), the net change in loading on the flat plate is different as shown in Fig. 9. Also, these two centerline

load distributions (obtained with and without external flow) suggest that the moments would be significantly different. In the case of the external flow condition, the pressure differential or surface loading was referenced to the pressure distribution generated on the flat plate with the plume generator off and located at a y/d_e value of 2.5. The assumption was made that this pressure distribution would not change significantly with a variation in y/d_e from 2.5 to 3.75. For the case with no external stream, the pressure differential was referenced to the quiescent environment pressure [p_w (p_{o_j} = 0) = p_b].

A summary of the graphically integrated experimental and theoretical centerline pressure distributions is presented in Table VI and shown graphically in Fig. 10. These integrated pressure distributions represent local centerline loading factors produced by the impinging plume flow on the flat plate. The limits of the integration as indicated in Table V extend from 2 in. upstream to 10 in. downstream of the nozzle exit plane (i.e., a hypothetical flat plate 1 ft long). As noted previously for the case of a plume expanding into a quiescent environment (M_∞ = 0), the agreement between the predicted and experimental plume impingement loading is fairly good with differences of 15 percent or less for these test conditions. For the case pertaining to an external stream, the predicted values are significantly smaller than the experimental values.

A comparison of the load factors obtained with and without an external stream for these plume conditions indicates that the plume-induced impingement loading with the external stream is more than three times larger. In this particular comparison at these test conditions, most of this difference in the loading factor could be attributed to the difference between the plume boundary pressure (p_b) for the case without external flow to the free-stream static pressure for the case with external flow. A higher quiescent plume boundary pressure was required to keep the size and shape of the initial portion of the expanding plume in a quiescent environment equal to the plume which was formed in the Mach number 18 external stream. However, in a quiescent environment, if the plume boundary pressure is reduced to the free-stream static pressure of the Mach number 18 external flow field, theoretically the plume size would increase; the plume impingement point would move upstream along the flat plate surface; and, based on the inviscid theoretical plume calculations, the maximum or peak impingement pressure would increase. In any case for these test conditions, the presence of the external stream can cause a significant change in the resultant impingement loading on the flat plate.

The heat-transfer-rate distributions generated by the impinging helium plume on the flat plate in the presence and absence of an external stream are shown in Fig. 11. The Stanton number is defined in terms of the helium plume mass flow rate and total enthalpy. In general, the trends in the heat-transfer rates are similar to the trends observed in the plume impingement pressure distributions. However, while the peak heat-transfer rate decreased as the plate was displaced further (vertically) from the plume axis in a quiescent environment (Figs. 11a and b), this trend was reversed when the external stream was present. The presence of the external stream also caused the peak heat-transfer rates to increase; compare Figs. 11c and d.

The general shape of the spanwise plume impingement heat-transfer and pressure distributions on the flat plate with and without external flow are shown, respectively,

in Figs. 12 and 13. These distributions are presented in the form of lines of constant heat-transfer rates and lines of constant pressure (isopiestic lines). Superimposed on these results is the theoretical estimate of the intersection of the inviscid plume boundary with the flat plate. In general, the loadings produced in the absence of an external stream generate lines of constant pressure and heat transfer which originate on the flat plate centerline and extend outward over the plate surface and then return to the center of the load distribution.

In the case with the external stream (Fig. 13), the line denoting the theoretical intersection of the plume with the plate is more nearly parabolic in shape. Although the lines of constant pressure form closed loops originating and, in most cases, terminating on the centerline of the impingement loading, some of the heat-transfer-rate lines do not form closed loops. For example (see Fig. 13a), some peak heat- transfer rates are generated off-axis and outside of the theoretical plume impingement boundary. This is consistent with the trend in the centerline data previously noted in that the peak heat-transfer rates tended to increase as the surface was displaced further from the plume axis. Although additional test data may be required to confirm this trend, these results indicate that the deflection of the external stream by the plume toward the plate can cause an increase in the heat-transfer rates which differ from the rates produced when the plume expands into a quiescent environment.

Figures 14 and 15 are plots of the heat-transfer-rate and pressure distributions across the span of the flat plate at various model stations. In the absence of an external stream and along the centerline (Fig. 14), the heat-transfer rate and pressure decay) and also at each of the succeeding model stations, higher peak heat-transfer rates occur outboard of the centerline. A similar trend is observed in the distributions presented for the case with external flow (Fig. 15) except that the heat-transfer rates were larger and the peak off-axis heat-transfer rate increased slightly at each successive model station (x/d_e value). Apparently this outboard, or off-axis, heat-transfer rate must eventually decay somewhere aft of the x/d_e model station of 12.5 and outboard of the spanwise coordinate z'/d_e of 8.25. No heat-transfer gages were located beyond z'/d_e value of 8.25.

SECTION V
CONCLUDING REMARKS

The observable effects of the external stream on the plume impingement loading were as follows:

1. The local pressure distribution in the immediate vicinity of the intersection of the plume boundary with the flat plate was not influenced by the external stream.

2. If the internal distribution of the plume properties and the plume size are nominally the same, then the net change in loading imposed on the flat plate is significantly altered by the presence of the external stream.

3. In the present tests, the local heat-transfer rates were significantly higher in the region where the plume boundary intersected the flat plate when the external stream was present. Peak heating occurred off-centerline.

Since these results indicate that plume impingement effects are significant and should be simulated in the presence of an external stream, the Captive Trajectory System now under development for Wind Tunnels A, B, and C should have the capability to supply high pressure gases to the model for plume simulation.

REFERENCES

1. Wojciechowski, C. J., Penny, M. M., and Frozen, R. J. "Space Shuttle Vehicle Rocket Plume Impingement Study for Separation Analysis." LMSC/HREC D162657, November 1970.

2. Norman, W. S., Kinslow, M., and Lewis, J. W. "Experimental Study of Simulated High Altitude Rocket Exhaust Plumes." AEDC-TR-71-25, July 1971.

3. Gardon, R. "An Instrument for the Direct Measurement of Intense Thermal Radiation." The Review of Scientific Instruments, Vol. 24, No. 5, May 1953, pp. 366 - 370.

4. Rudman, S. and Rubin, S. G. "Hypersonic Viscous Flow over Slender Bodies with Sharp Leading Edges." AIAA Journal, Vol. 6, No. 10, October 1968, pp. 1883 - 1890.

5. Prozan, R. J. "Development of a Method of Characteristics Solution for Supersonic Flow of an Ideal, Frozen, or Equilibrium Reacting Gas Mixture." LMSC/HREC A782535, April 1966.

APPENDIXES

I. ILLUSTRATIONS

II. TABLES

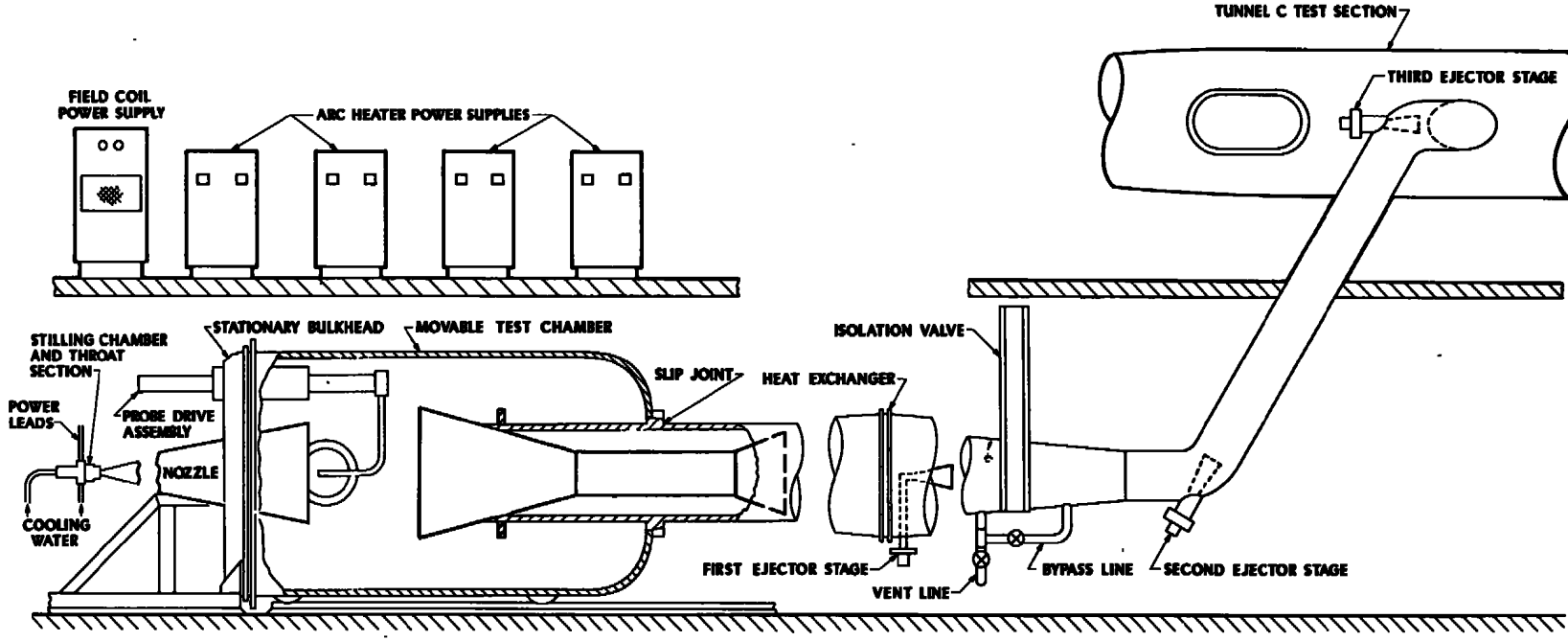

Fig. 1 Tunnel M Test Unit

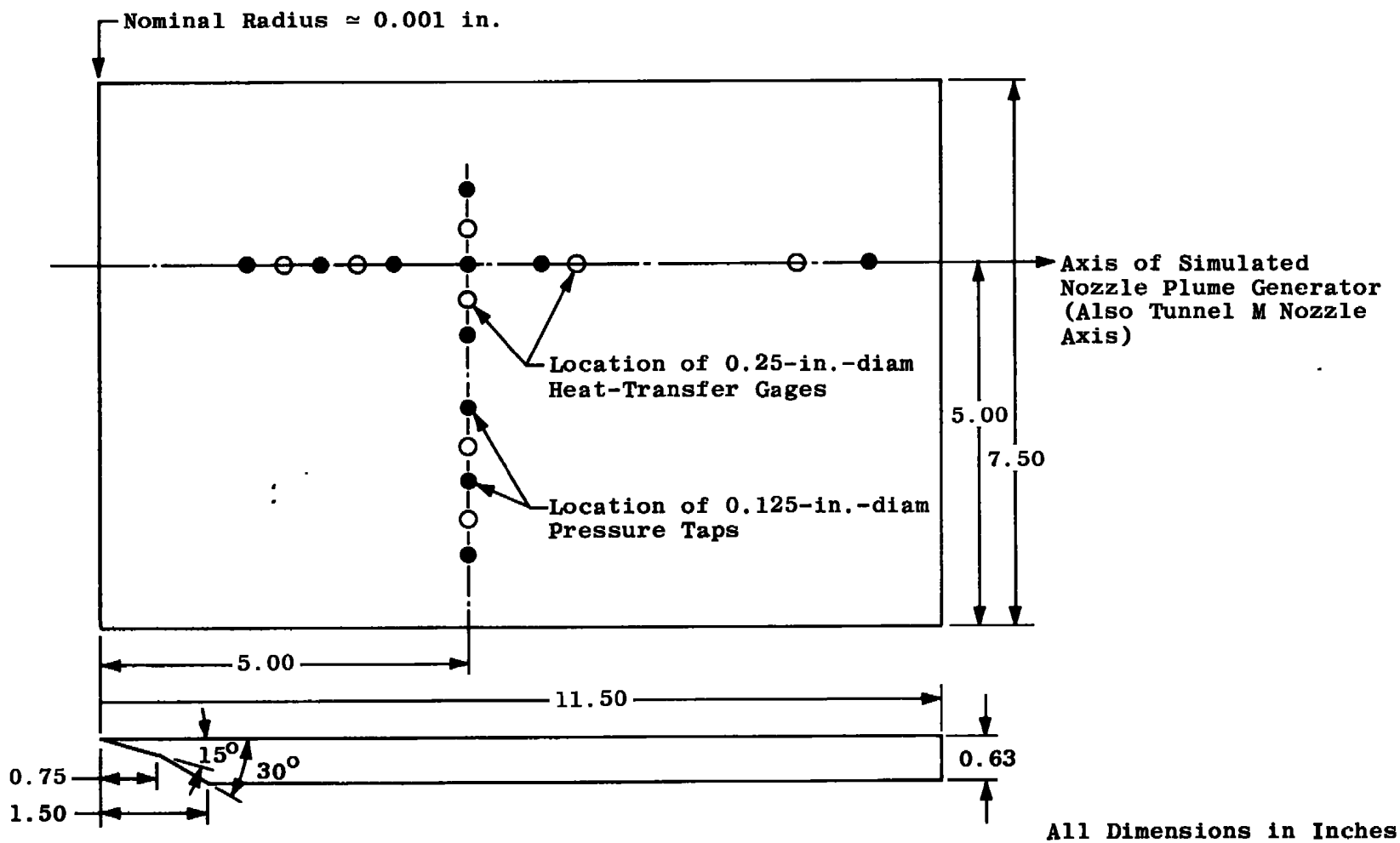

a. Instrumentation Locations

Fig. 2 Flat Plate Plume Impingement Model

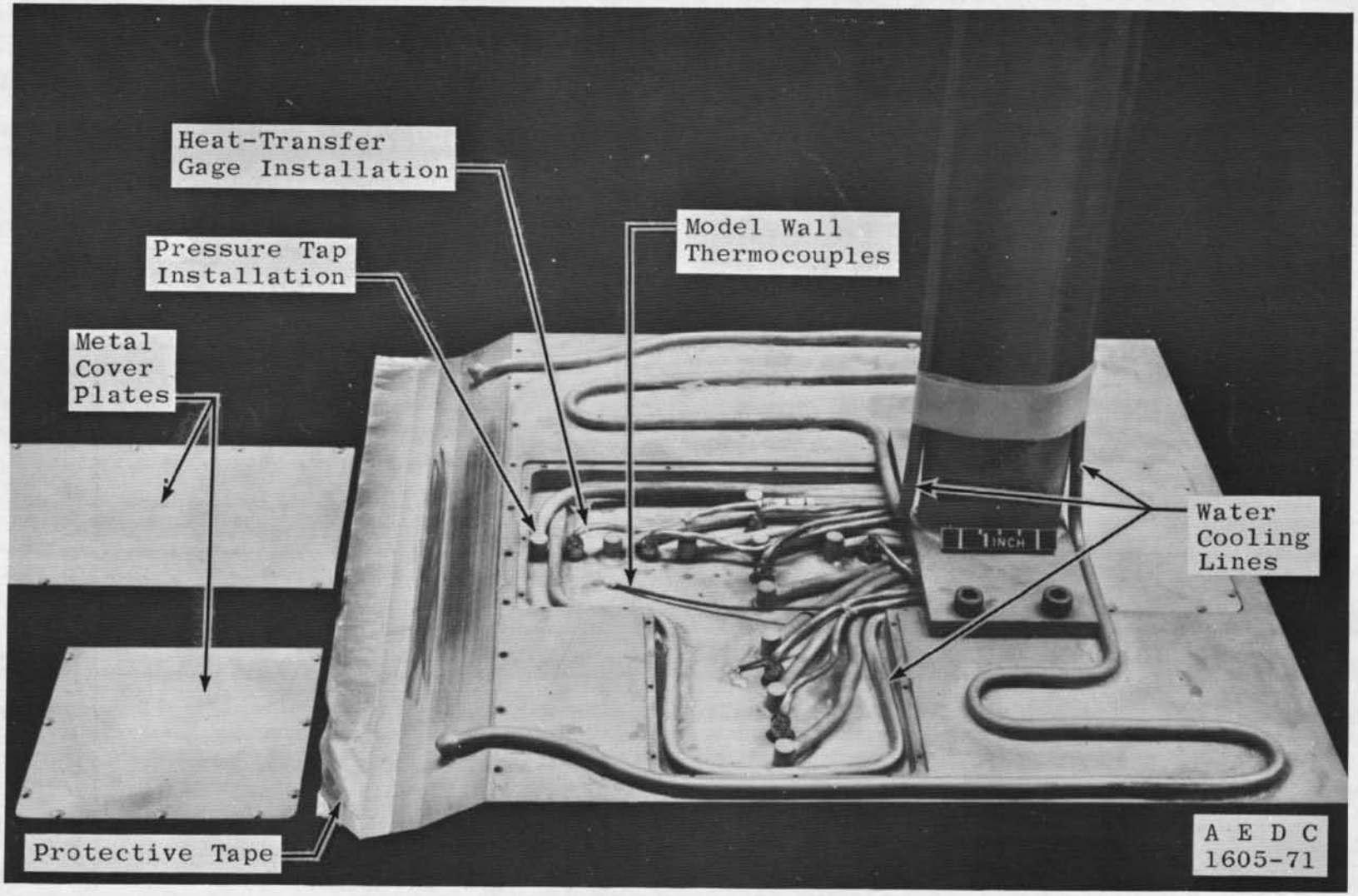

b. Model Photograph (Bottom View)
Fig. 2 Concluded

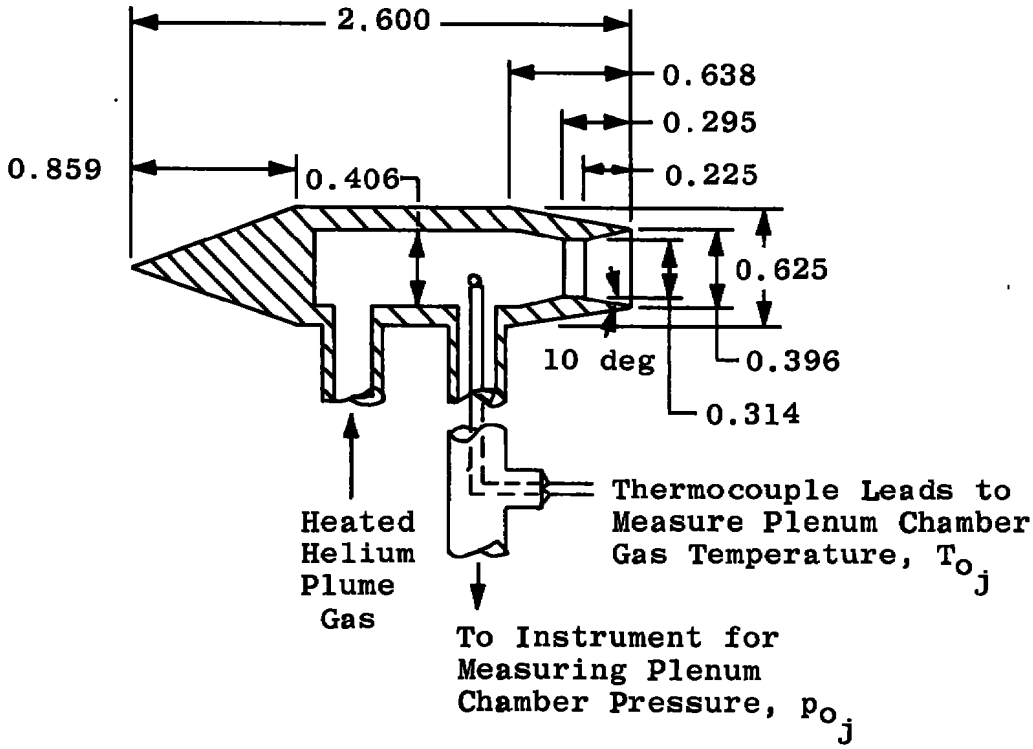

a. Plume Generator

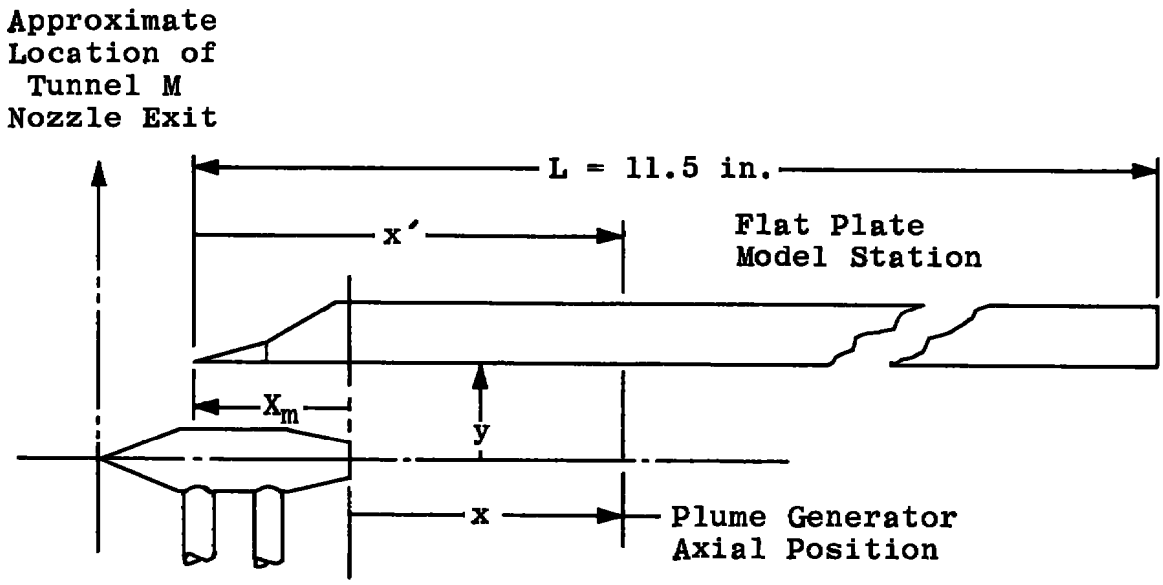

b. Coordinate System

Fig. 3 Plume Generator and Coordinate System for the Test Program

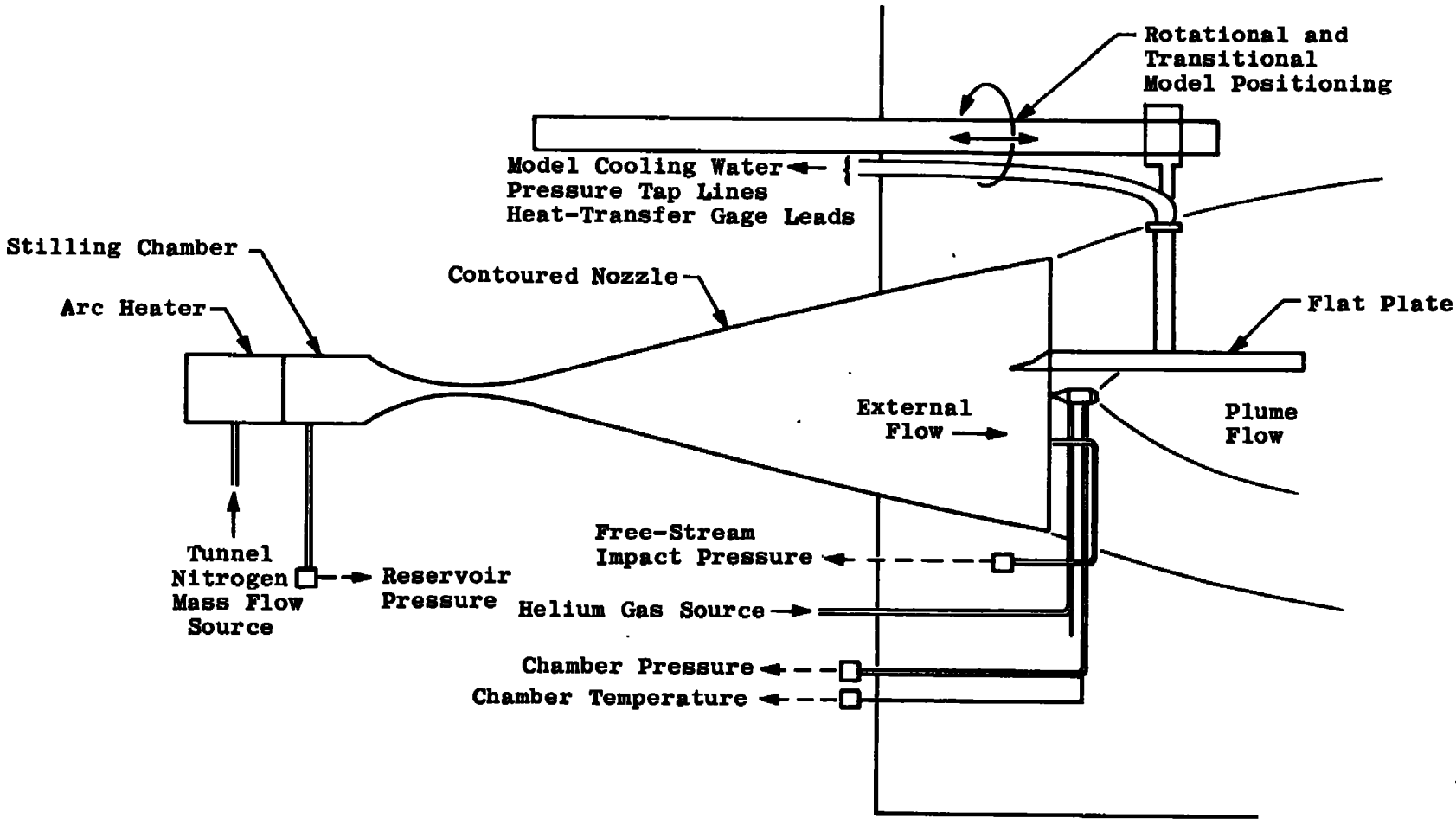

a. Schematic

Fig. 4 Test Installation

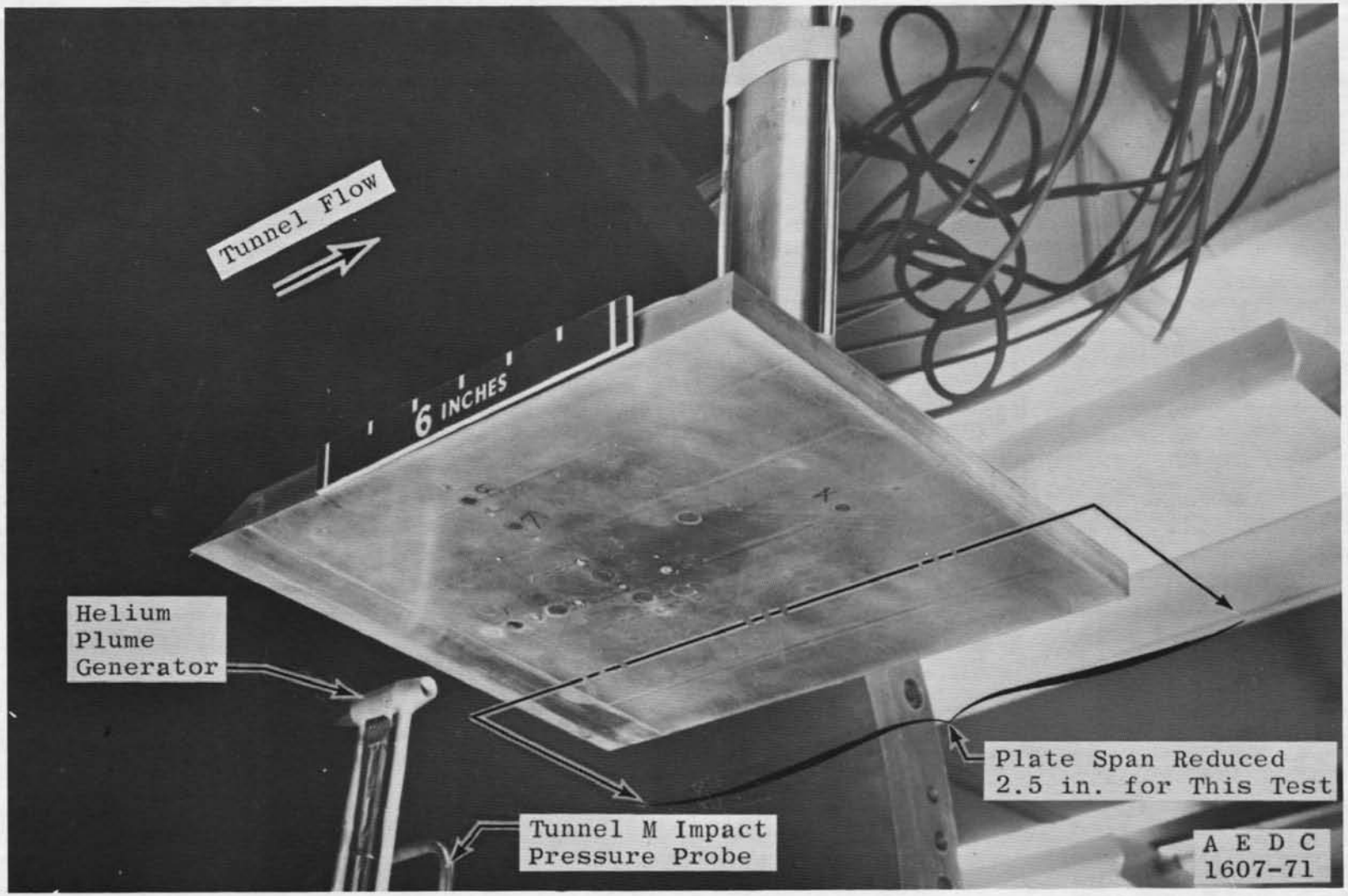

b. Photograph

Fig. 4 Concluded

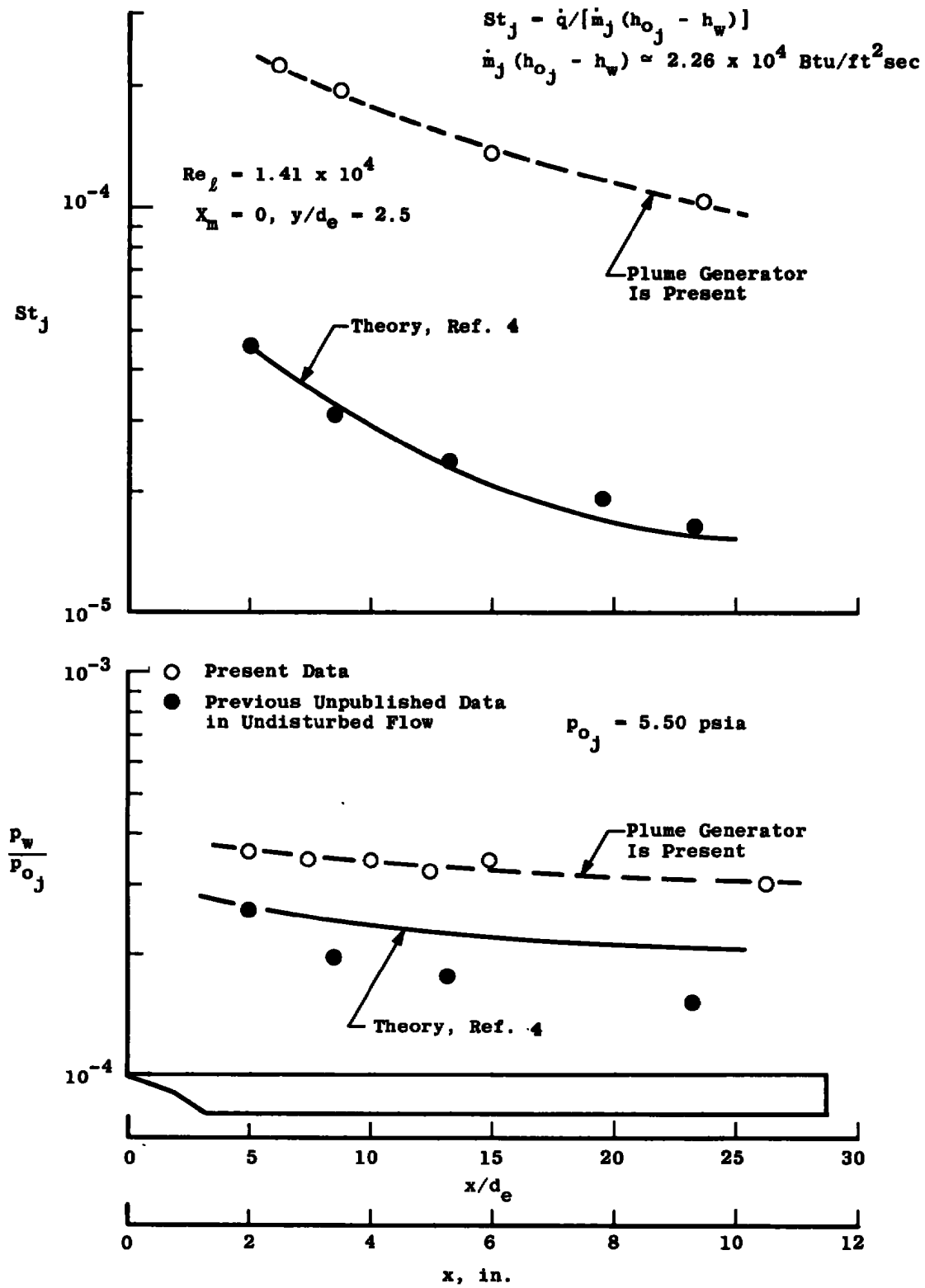

Fig. 5 Pressure and Heat-Transfer-Rate Distributions on the Flat Plate in a Mach Number 18.2 Stream, $Re_\ell = 1.41 \times 10^4$ ($X_m = 0$ and $y/d_e = 2.5$)

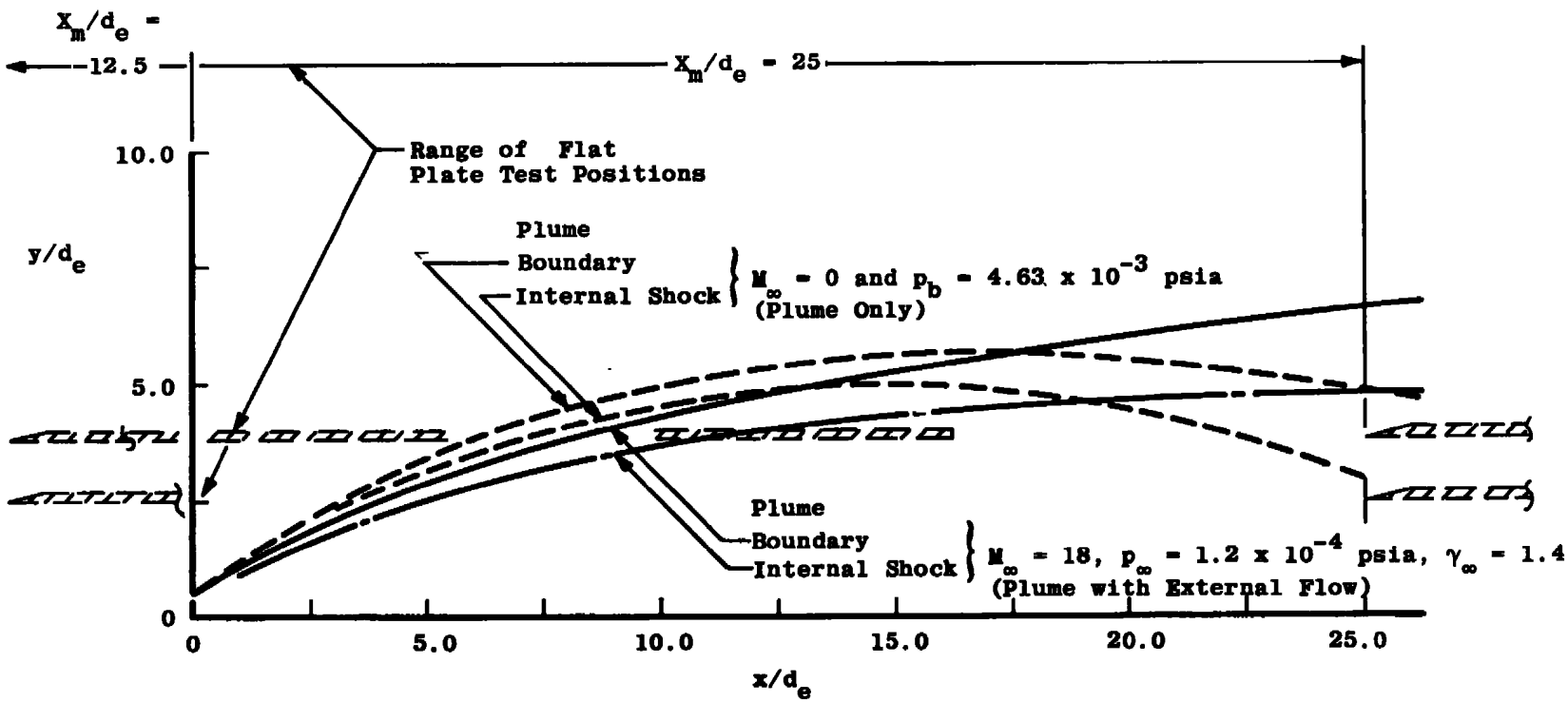

Fig. 6 Theoretical Helium Plume (γ_j = 1.67) Boundary with and without External Flow, A/A* = 1.61, M_j = 2.073 and p_{o_j} = 5.56 psia

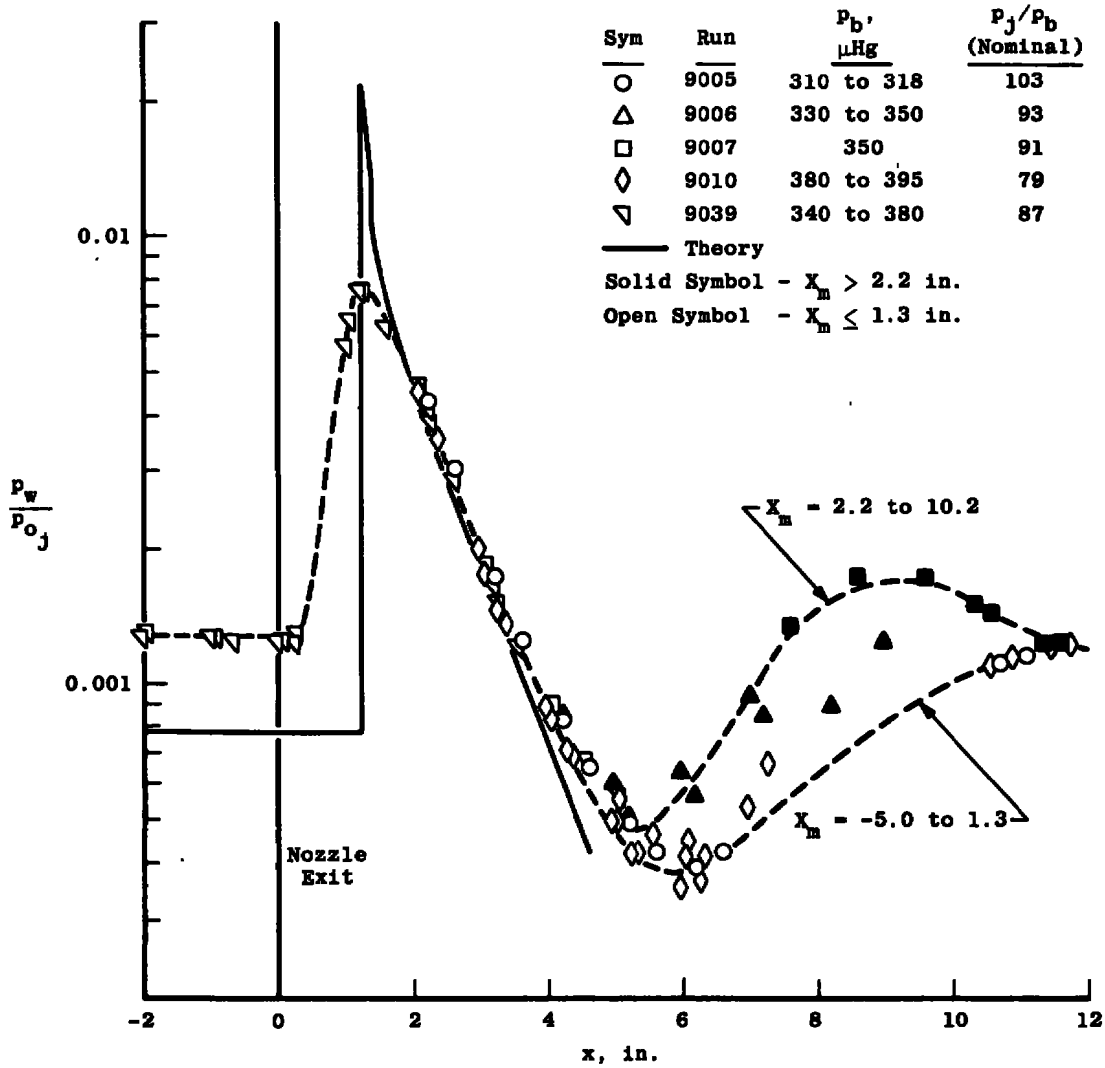

a. No External Flow ($M_\infty = 0$) $y/d_e = 2.5$

Fig. 7 Centerline Plume Impingement Pressure Distributions on a Flat Plate, $A/A^* = 1.61$, $M_j = 2.073$ and $p_{o_j} = 5.56$ psia

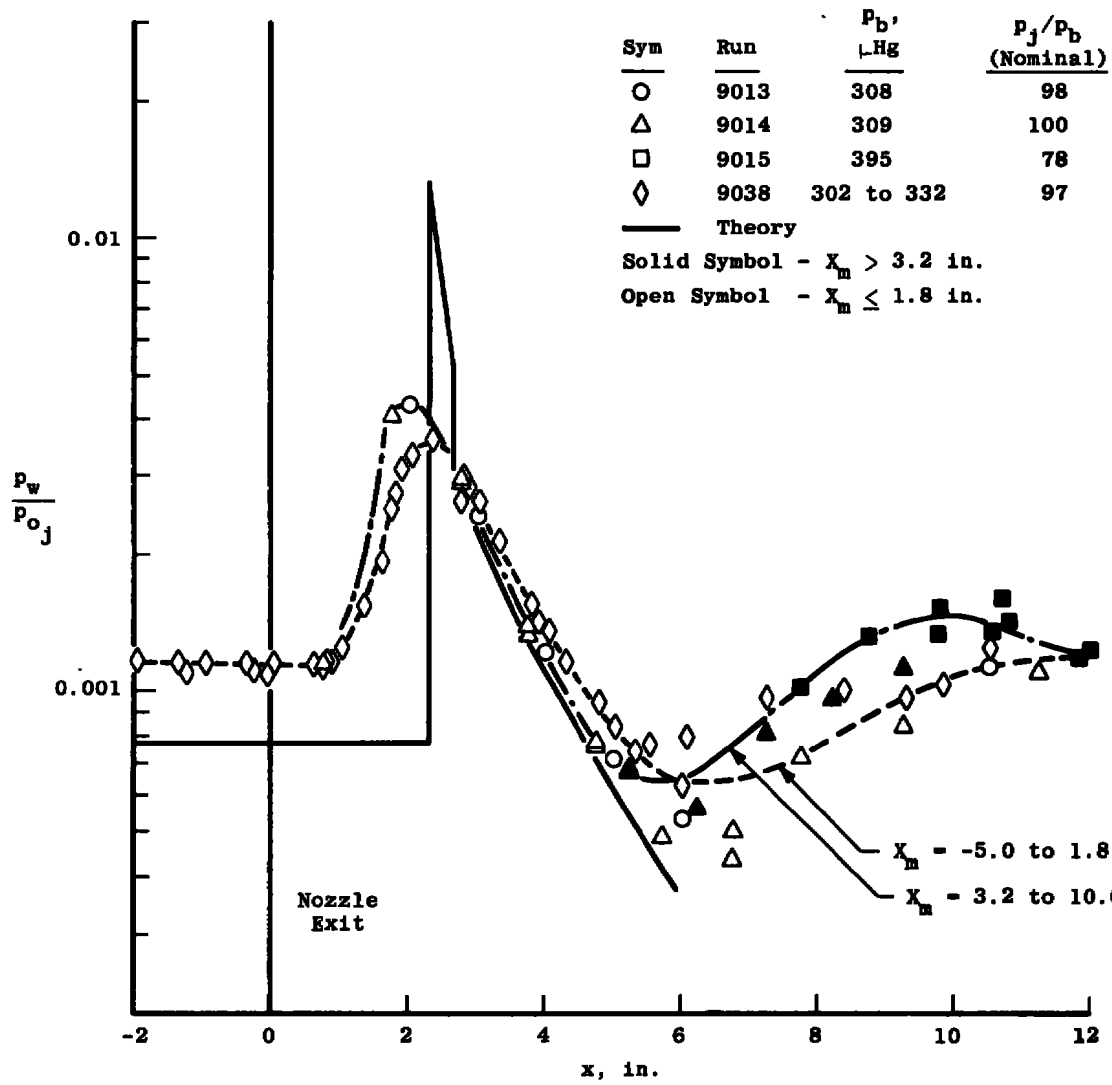

b. No External Flow ($M_\infty = 0$), $y/d_e = 3.75$
Fig. 7 Continued

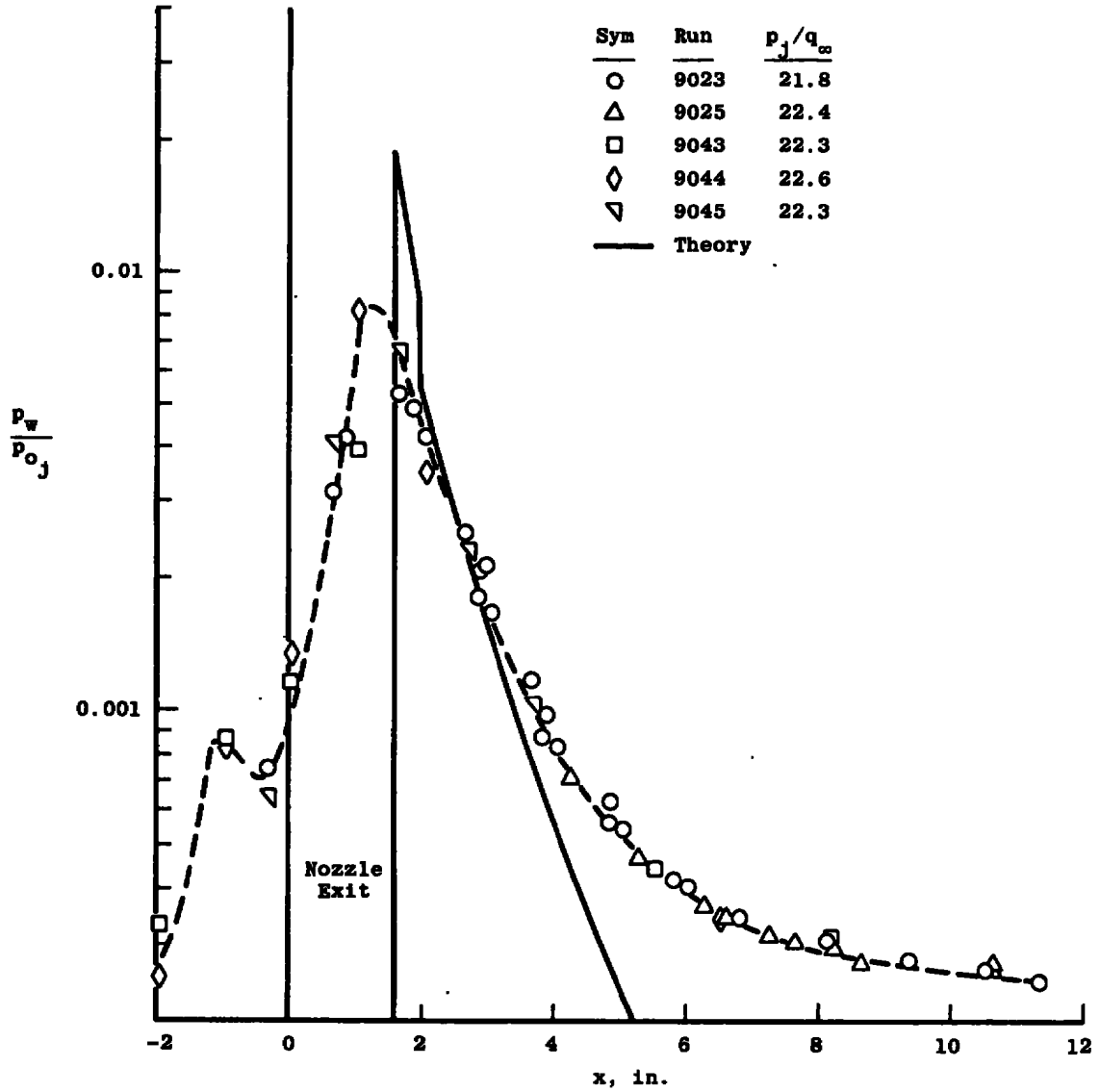

c. External Flow (M_∞ = 18 and Re_ℓ = 1.41 x 10^4), y/d_e = 2.5
Fig. 7 Continued

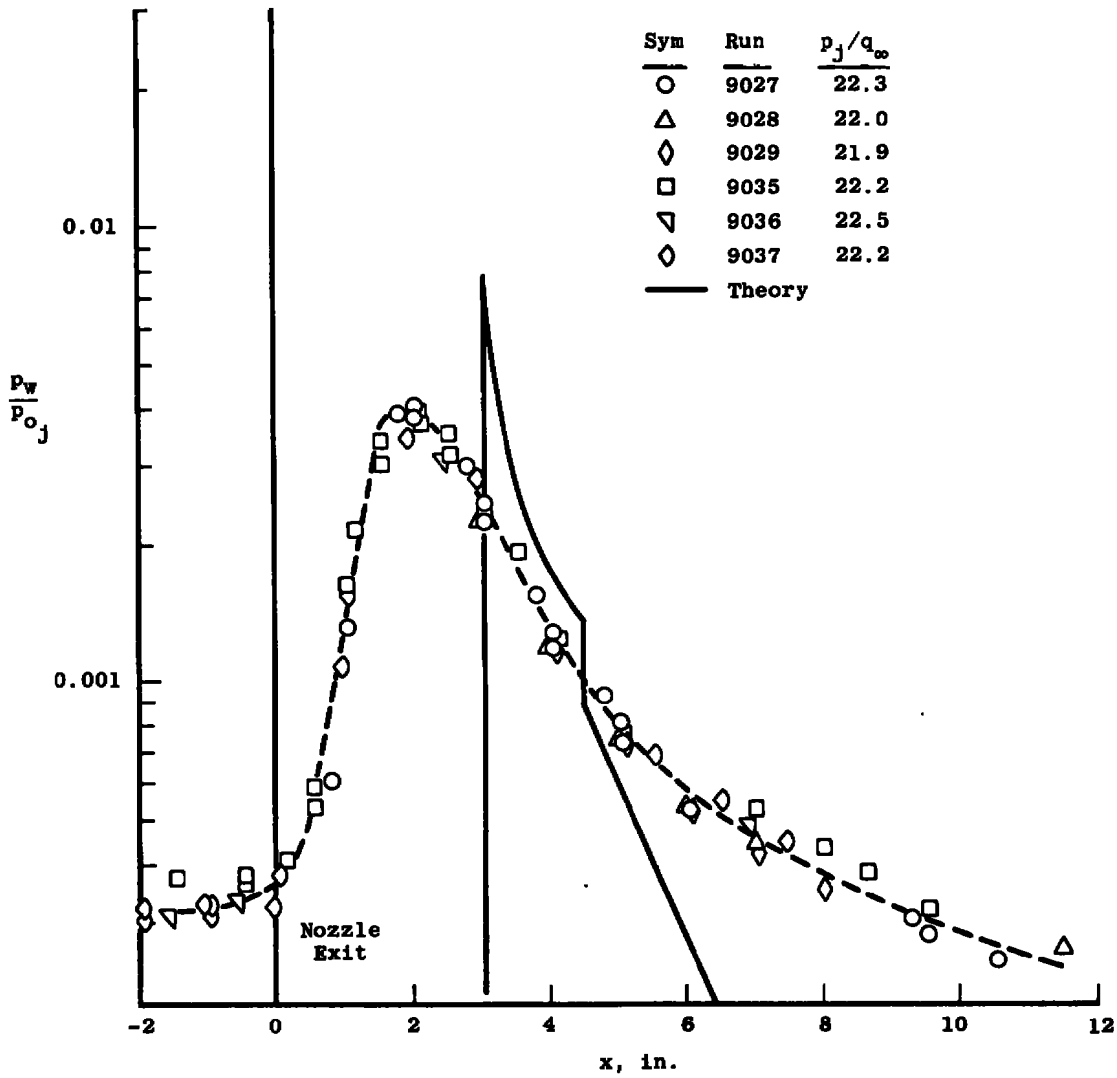

d. External Flow (M_∞ = 18 and Re_ℓ = 1.41 x 10^4), y/d_e = 3.75

Fig. 7 Concluded

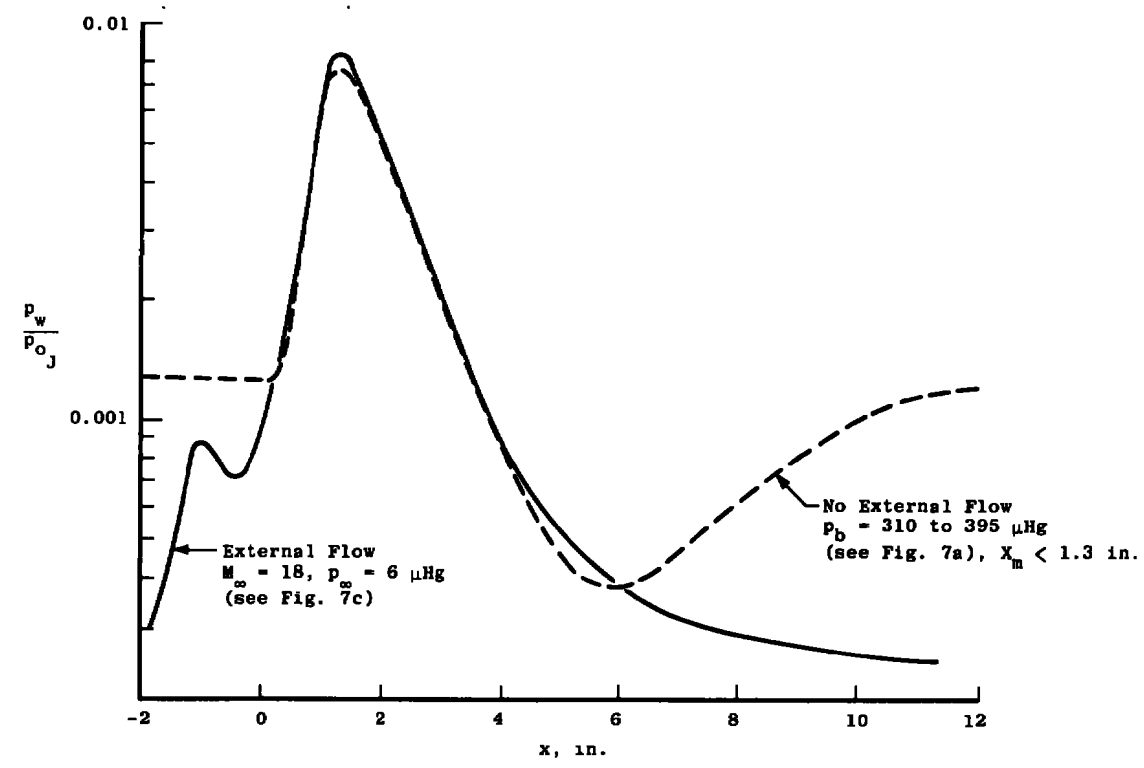

a. y/d_e = 2.5

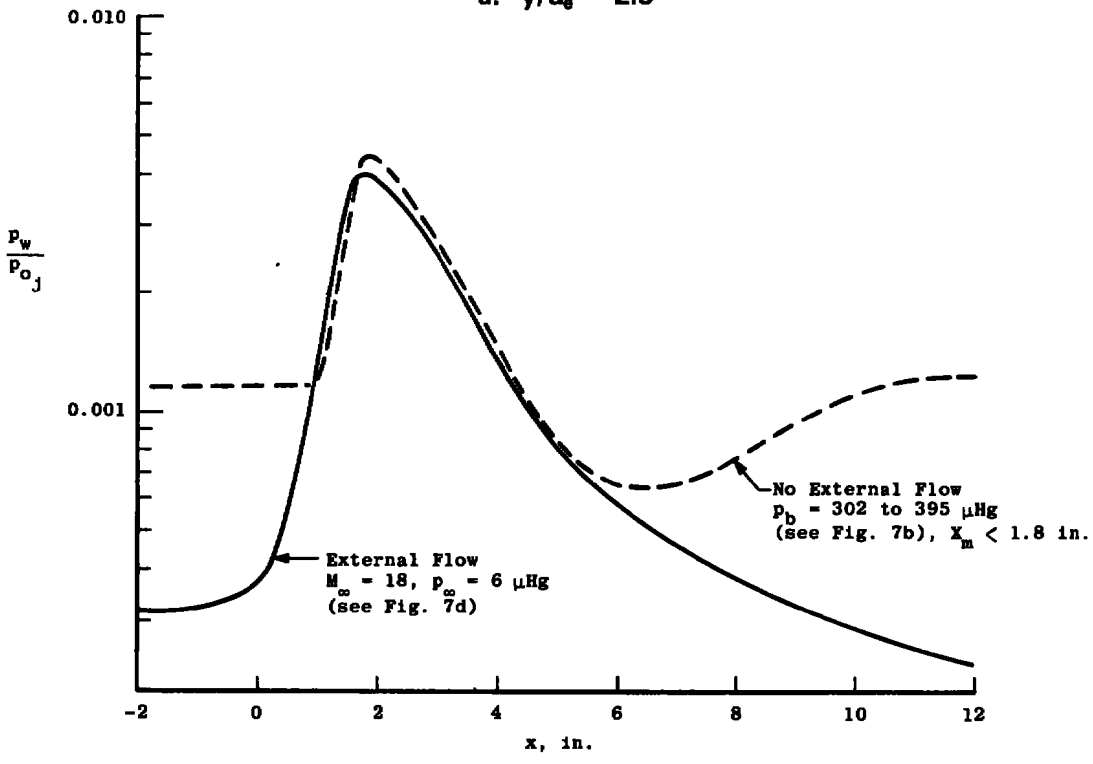

b. y/d_e = 3.75

Fig. 8 External Flow-Field Effects on the Plume Impingement Pressure Distribution

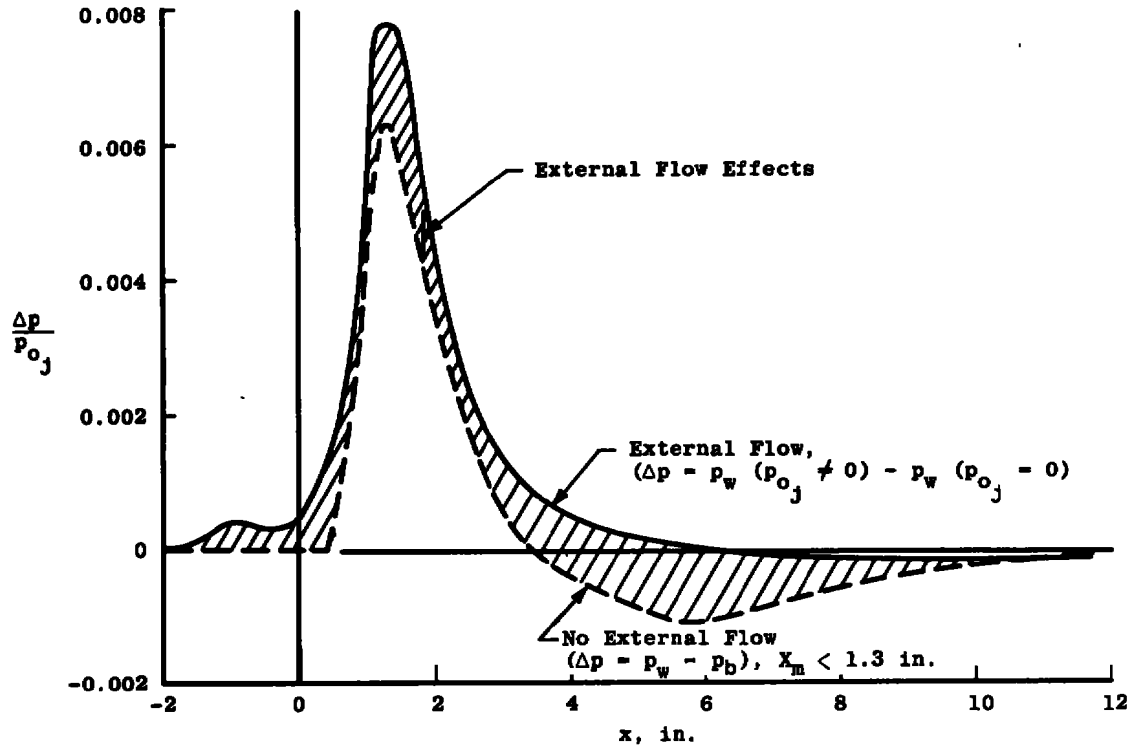

a. $y/d_e = 2.5$

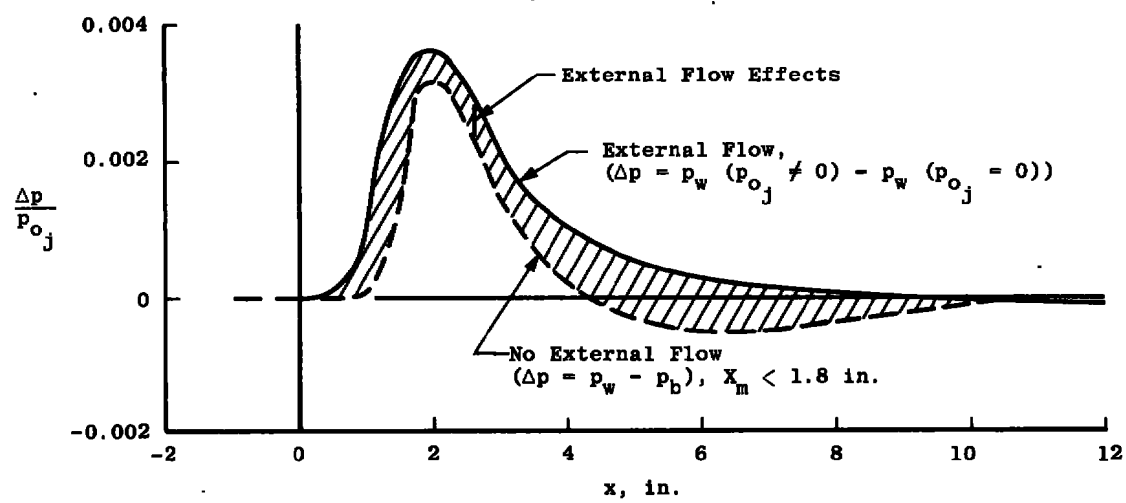

b. $y/d_e = 3.75$

Fig. 9 The Centerline Plume Impingement Load Distribution

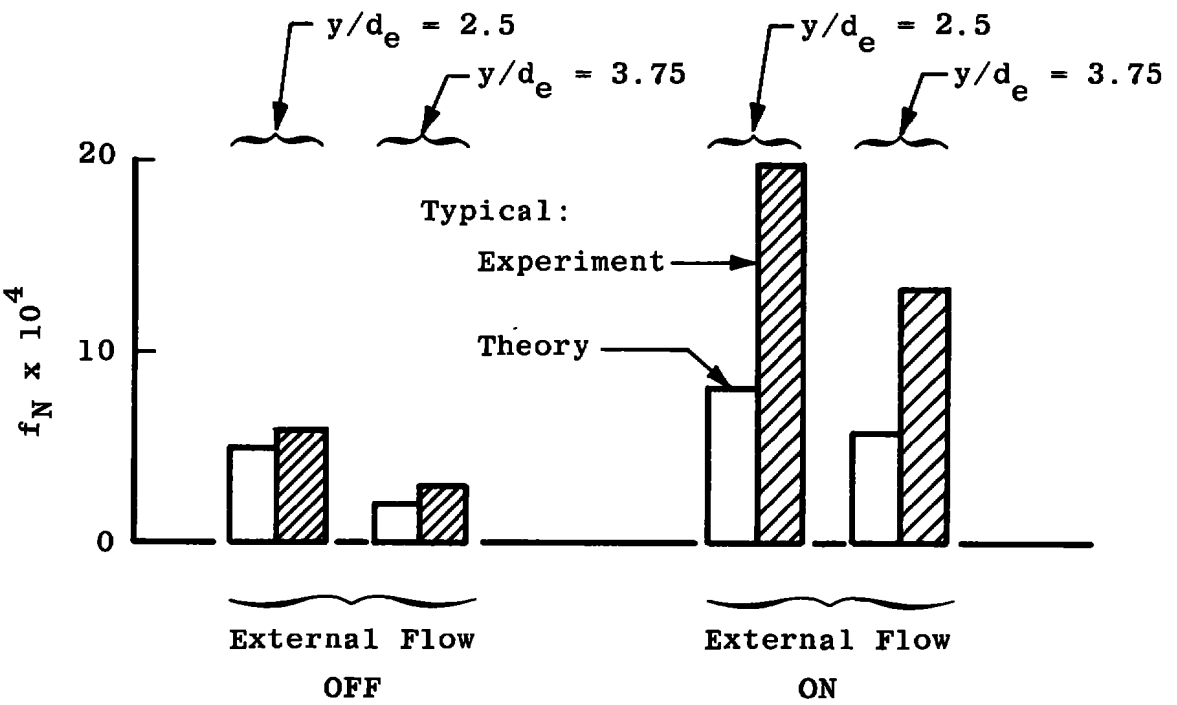

Fig. 10 Comparison of Theoretical and Experimental Centerline Plume Impingement Loading Factors

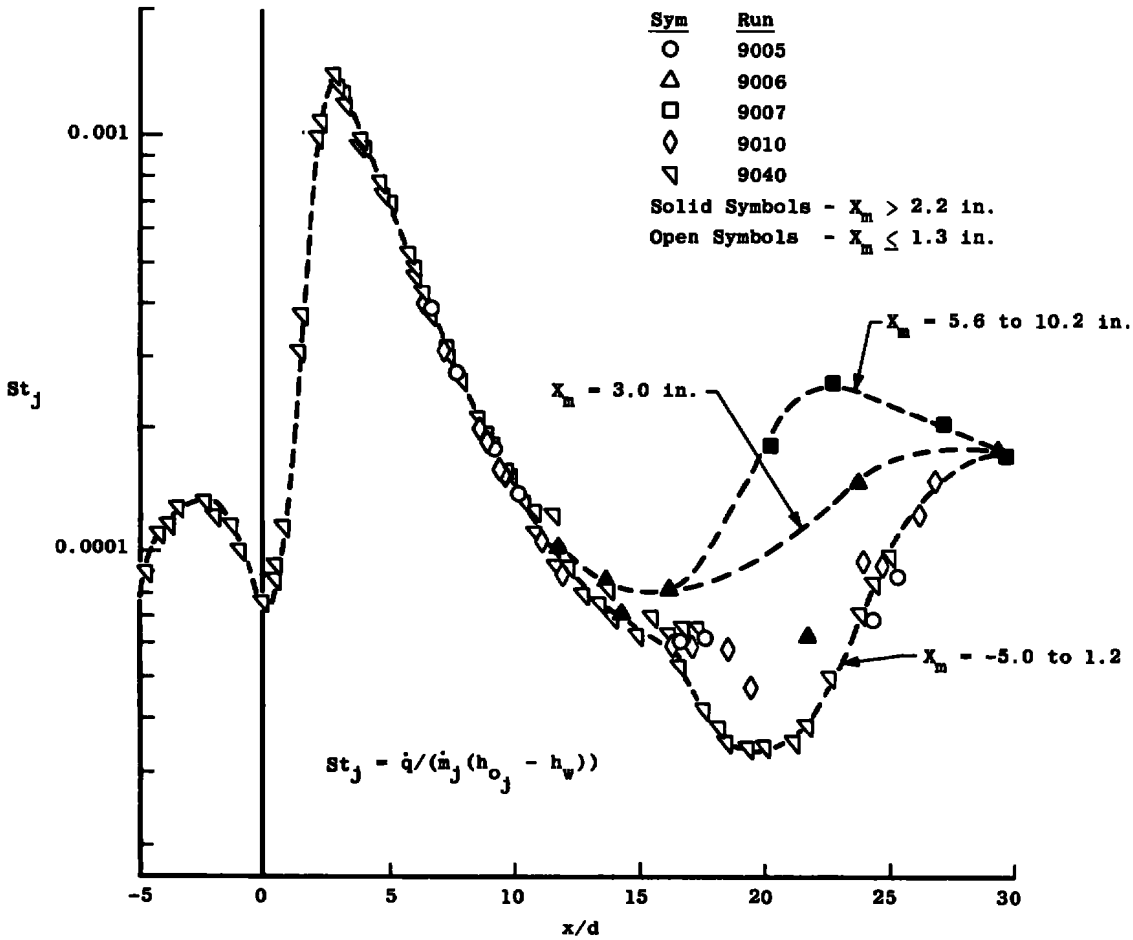

a. No External Flow ($M_\infty = 0$), $y/d_e = 2.5$

Fig. 11 Centerline Plume Impingement Heat-Transfer-Rate Distributions on the Flat Plate, $A/A^* = 1.61$, $M_j = 2.073$, $p_{o_j} = 5.56$ psia, $T_{o_j} \simeq 680°K$, and $T_w \simeq 315°K$

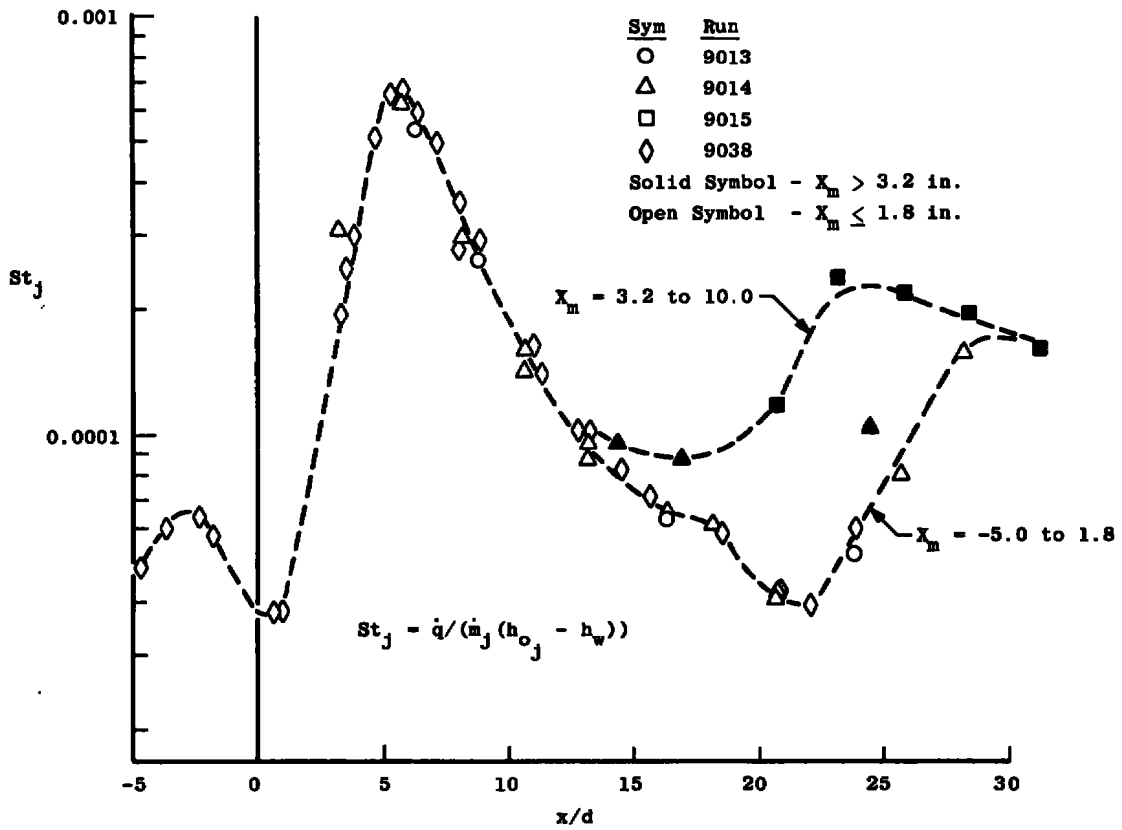

b. No External Flow ($M_\infty = 0$), $y/d_e = 3.75$
Fig. 11 Continued

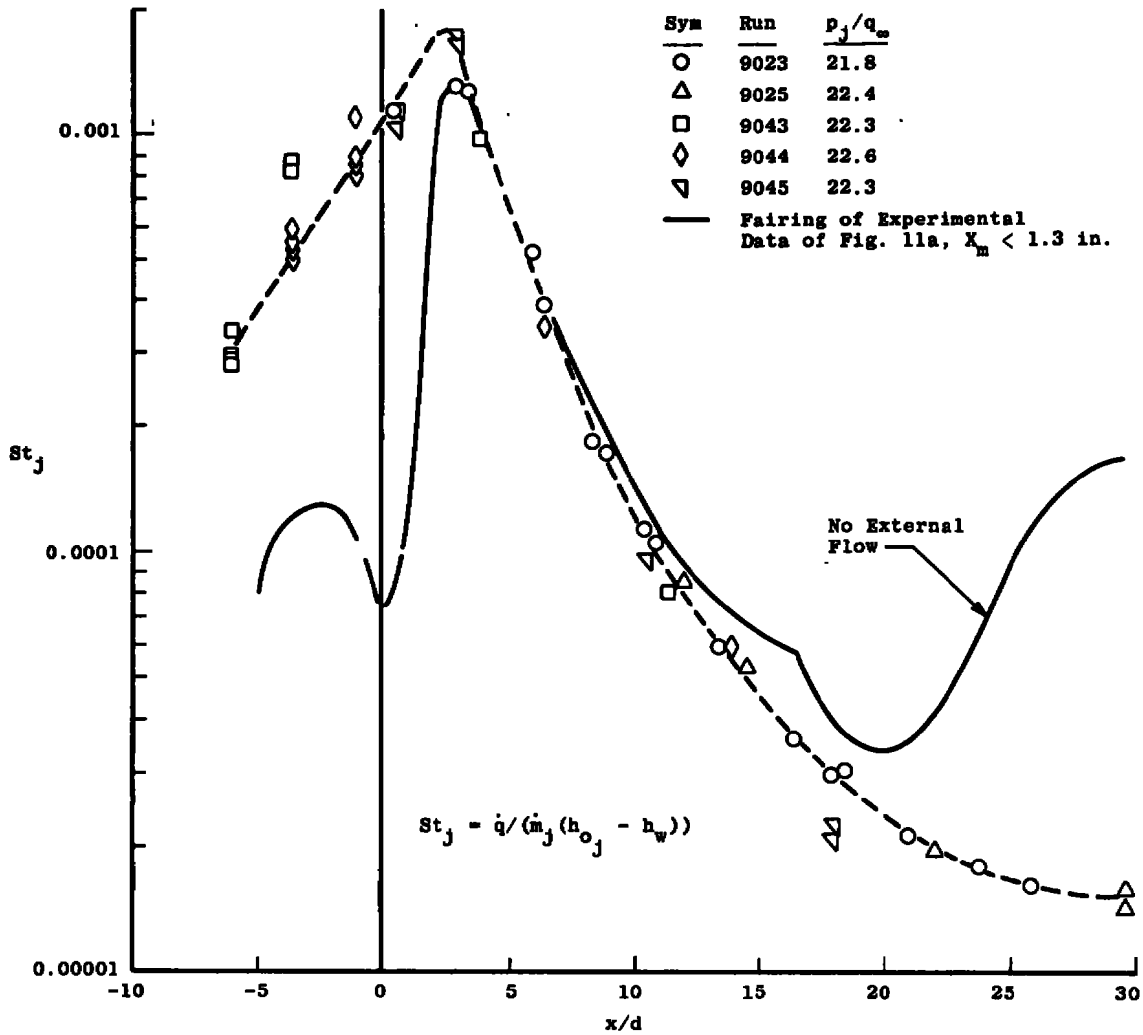

c. External Flow (M_∞ = 18 and Re_ℓ = 1.41 x 10^4), y/d_e = 2.5
Fig. 11 Continued

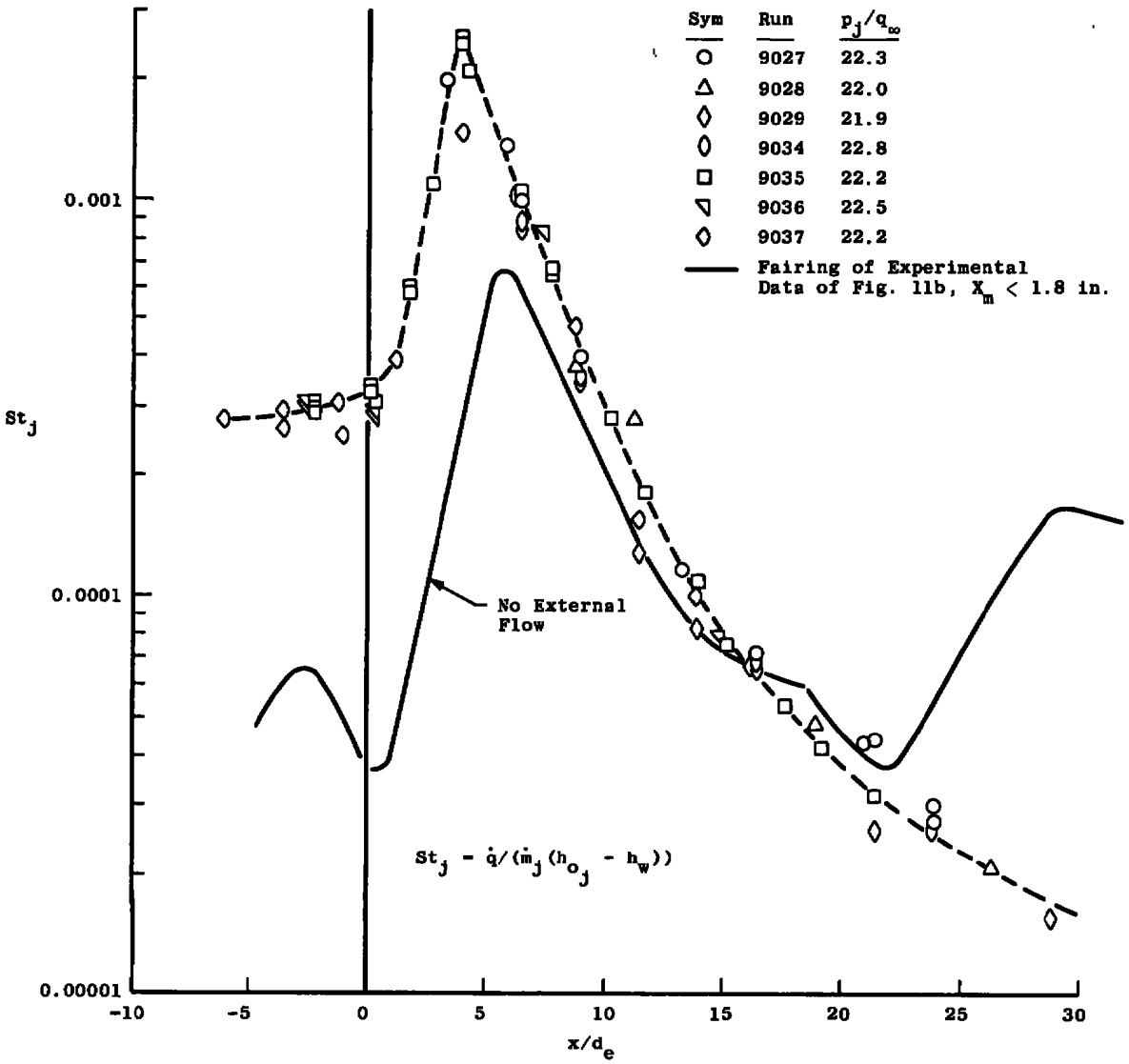

d. External Flow (M_∞ = 18 and Re_ℓ 1.41 x 10^4), y/d_e 3.75
Fig. 11 Concluded

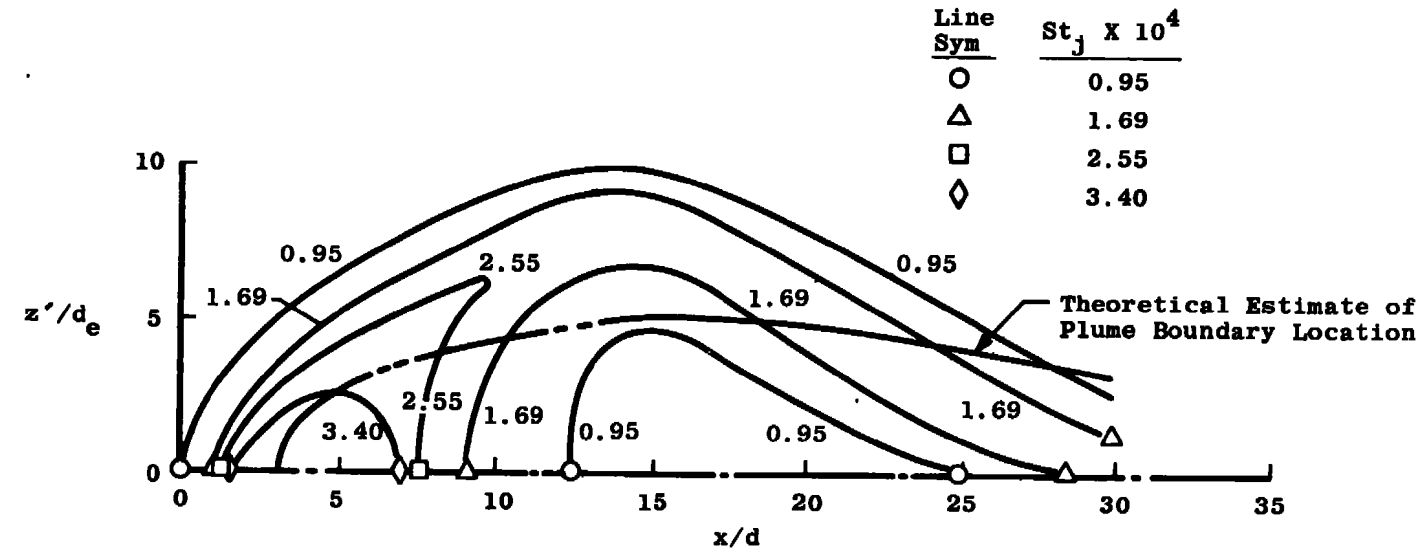

a. Isothermal Flux Lines

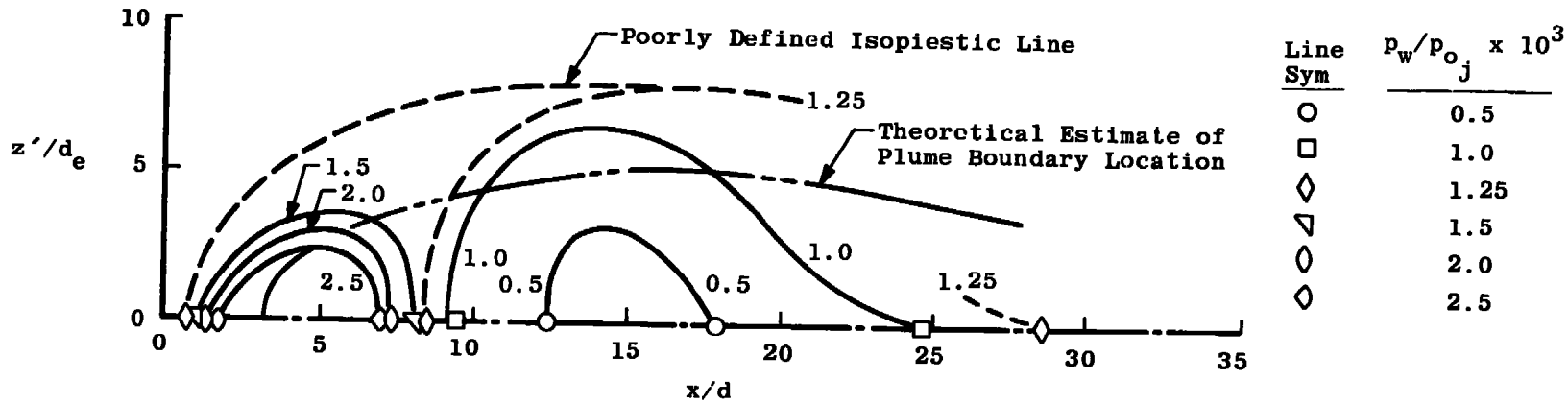

b. Isopiestic Lines

Fig. 12 Isolines of Plume Impingement Heat-Transfer Rate and Pressure Loading on a Flat Plate in a Quiescent Environment ($p_b \simeq 315$ to 395 μHg)

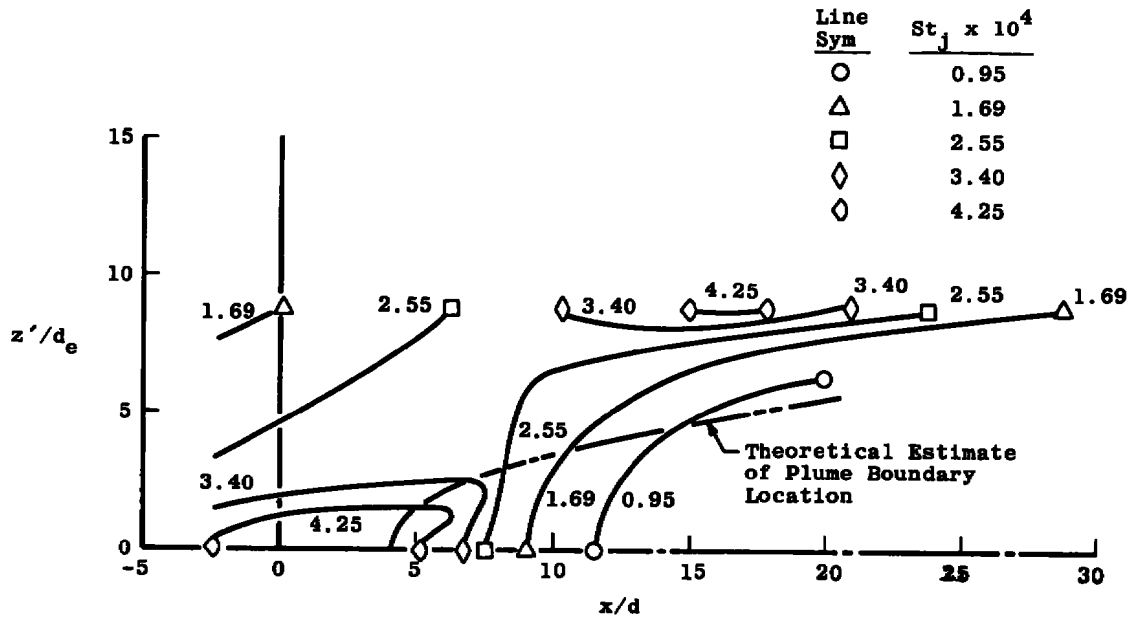

a. Isothermal Flux Lines

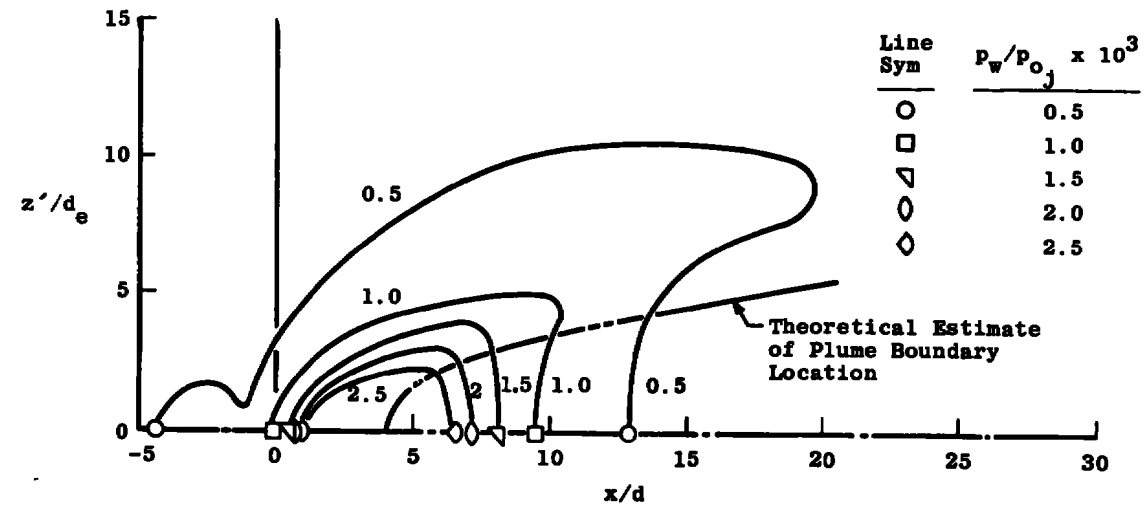

b. Isopiestic Lines

Fig. 13 Isolines of Plume Impingement Heat-Transfer Rate and Pressure Loading on a Flat Plate in an External Stream (M_∞ = 18.2 and p_∞ = 6 μHg)

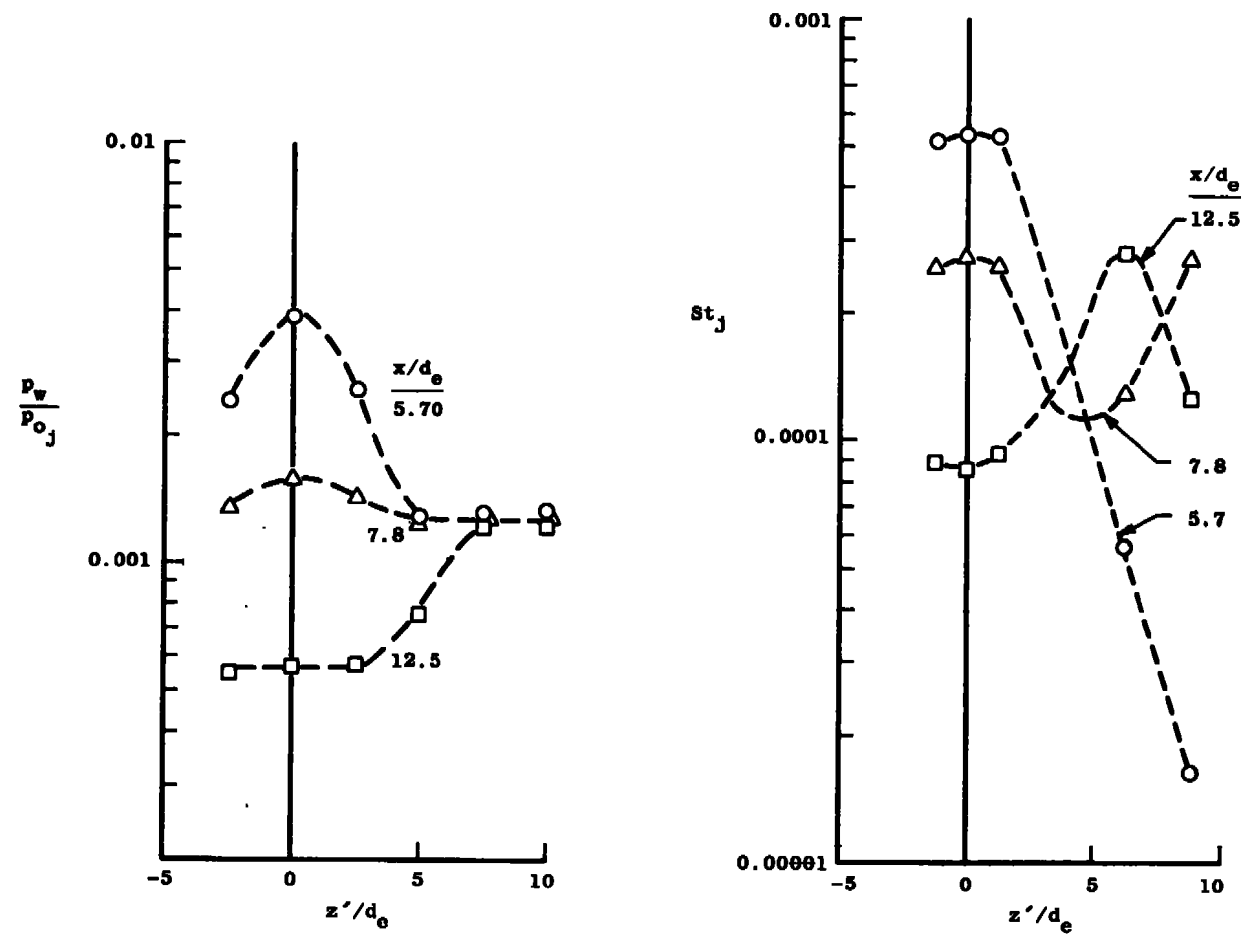

a. Pressure Distributions

b. Heat-Transfer-Rate Distributions

Fig. 14 Spanwise Plume Impingement Pressure and Heat-Transfer-Rate Distributions on the Flat Plate in a Quiescent Environment ($p_b \simeq 310$ to 395 μHg), $y/d_e = 2.5$

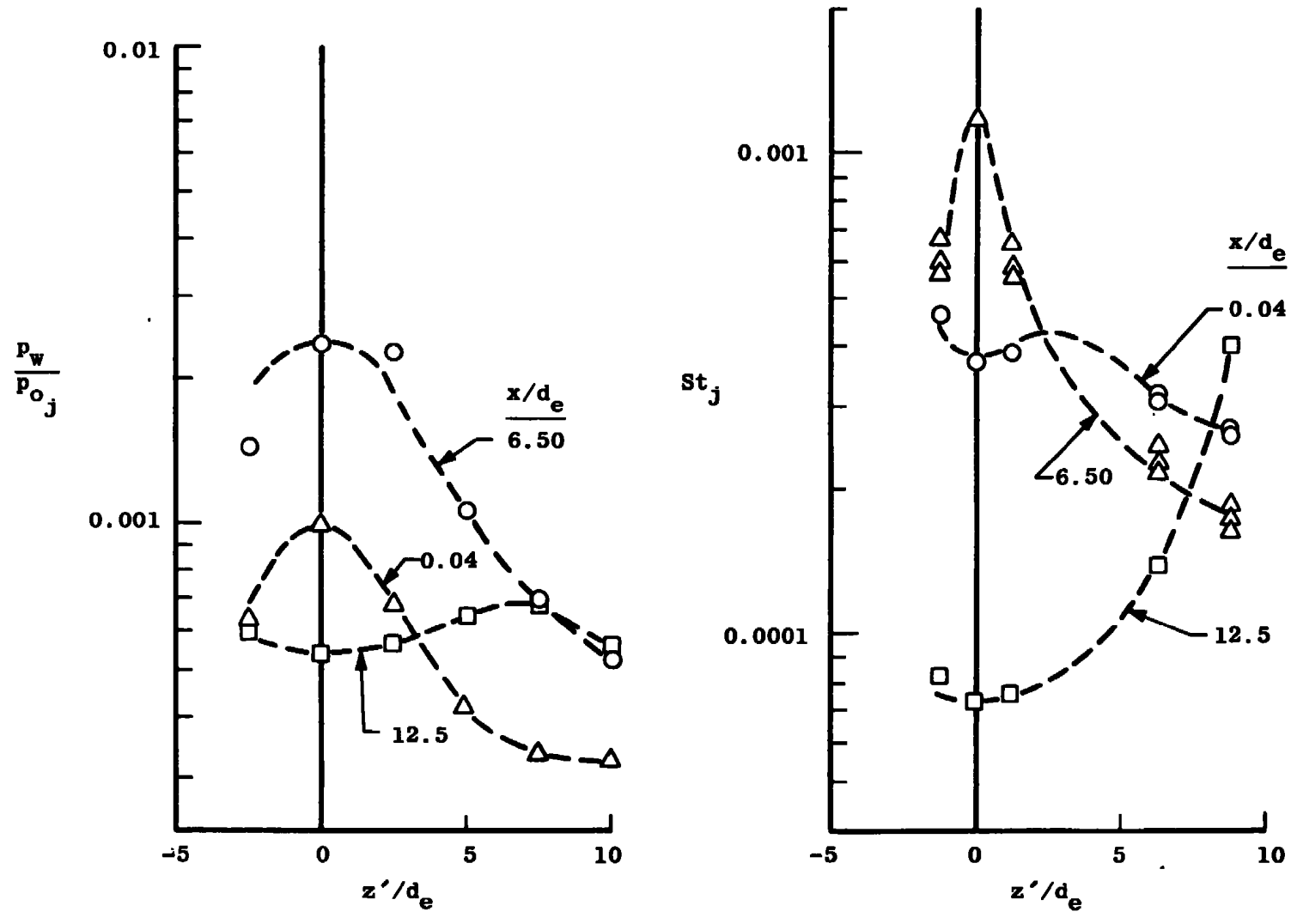

a. Pressure Distributions

b. Heat-Transfer-Rate Distributions

Fig. 15 Spanwise Plume Impingement Pressure and Heat-Transfer-Rate Distributions on the Flat Plate in an External Stream (M_∞ = 18.2), y/d_e = 2.5

TABLE I
REPEATABILITY OF TUNNEL STREAM PROPERTIES

Measurements:

Parameter	Repeatability	Percent
p_o	±1.5 psia	±0.5
$\dot{m}_\infty$	±0.001 lbm/sec	±2.0
p'_o	±100 μHg	±2.0

Inferred Values:*

T_o	±120°K	±4.0
M_∞	±0.26	±1.5
T_∞	±2.3°K	±5.0
p_∞	±0.6 μHg	±10.0
Re/in.	±92	8.0
$\rho_\infty u_\infty$	±1.6 x 10^{-5} lbm/(ft^2-sec)	8.0

*These values based on ideal gas relationships and a Taylor series propagation in the error.

TABLE II
REPEATABILITY OF TEST PARAMETERS

Parameter	Nominal Values	Repeatability	Percent Nominal Value
p_{o_j}	5.6 paia	±0.06 psia	±1.0
T_{o_j}	300°K	±3.0°K	±4.0
p_j	0.6 psia	±310 μHg	±1.0
p_w (min)	260 μHg	±10 μHg	±4.0
p_w (max)	2350 μHg	±20 μHg	±1.0
$\dot{q}$ (min)	0.36	±0.10 Btu/(ft^2-sec)	±28.0
$\dot{q}$ (max)	55.0	±1.50 Btu/(ft^2-sec)	±2.8
T_w	315°K	±5°K	±1.5
$\dot{p}_w/p_j$ (min)	0.0009	±0.000045	±5.0
St_j (min)	0.00001	±0.00000074	±7.0
p_j/q_∞	22.0	±1.6	±7.0

TABLE III
NOMINAL TUNNEL M CONTOURED NOZZLE OPERATING CONDITIONS WITH NITROGEN GAS

$\dot{m}_\infty$, lbm/sec	0.0515
p_o, atm	19.0 (279.0 psia)
T_o, °K	2900
h_o, Btu/lbm	1500
p'_o, mm Hg	2.55 (4.83×10^{-2} psia)
M_∞	18.2
Re/in.	1250 ($Re_\ell = 1.44 \times 10^4$)
p_∞, μHg	6.0 (1.16×10^{-4} psia)
T_∞, °K	45.0
u_∞, ft/sec	8165
λ_∞, in.	0.022
q_∞, lbf/ft^2	3.90 (2.71×10^{-2} psia)

TABLE IV
NOMINAL HELIUM PLUME GENERATOR OPERATING CONDITIONS

Parameter	Nominal Value	Simulated* Plume
A/A^*	1.61	25.0
$\dot{m}_j$, lbm/sec	0.0024	—
p_{o_j}, psia	5.56	440
T_{o_j}, °K	680	—
h_{o_j}, Btu/lbm	1520	—
γ_j	1.67	1.27
M_j	2.07	4.26
T_j, °K	280	—
p_j, psia	0.597	—
p_j/p_∞	5.15×10^3	—
p_j/q_∞	22.0	—

*The formulation of the similarity parameters which are a function of the plume size and momentum distribution is described in detail in Ref. 2. In this instance, the test program using helium gas simulates a plume at a pressure altitude of 262,000 ft.

TABLE V
TEST SUMMARY

y/d_e	X_m/d_e Range	Plume		External Stream	
		On	Off	On	Off
1.25*	-3.2 to 25.0	x			x
2.50	0		x	x	
2.50	-13.1 to 25.5	x			x
2.50	-12.5 to 25.0	x		x	
3.75	-12.5 to 25.0	x			x
3.75	-12.5 to 5.0	x		x	
5.00*	4.2 to 23.1	x			x

*Test data not discussed in this report.

TABLE VI
COMPARISON OF CENTERLINE PLUME IMPINGEMENT LOADING FACTORS

No External Flow, $M_\infty = 0$

$$f_N = \int_{-0.2L}^{L} \left(\frac{p_w - p_b}{p_{o_j}}\right) \cdot d\left(\frac{x'}{\ell}\right), \quad L = 10.0 \text{ in.}$$

y/d_e	f_N (Theory)	f_N (Experiment)	Percent Difference
2.5	4.84×10^{-4}	5.83×10^{-4}	12.0
3.5	2.02×10^{-4}	3.04×10^{-4}	15.0

External Flow, $M_\infty = 18.2$ and $(p_{o_j}/q_\infty) \simeq 210.0$

$$f_N = \int_{-0.2L}^{L} \left(\frac{p_w - p_\infty}{p_{o_j}}\right) d\left(\frac{x'}{L}\right), \quad L = 10.0 \text{ in.}$$

y/d_e	f_N (Theory)	f_N (Experiment)	Percent Difference
2.5	8.08×10^{-4}	19.7×10^{-4}	144.0
3.5	5.72×10^{-4}	13.3×10^{-4}	134.0

Note: $\Delta f_N = \int_{-0.2L}^{L} \left(\frac{p_w - p_\infty}{p_{o_j}}\right) \cdot d\left(\frac{x'}{\ell}\right) = 10.4 \times 10^{-4}$

Percent Difference = $([f_N \text{ (Exp.)}/f_N \text{ (Theory)}] - 1) \cdot 100$

UNCLASSIFIED
Security Classification

DOCUMENT CONTROL DATA - R & D

(Security classification of title, body of abstract and indexing annotation must be entered when the overall report is classified)

1. ORIGINATING ACTIVITY *(Corporate author)*
Arnold Engineering Development Center
ARO, Inc., Operating Contractor
Arnold Air Force Station, Tennessee

2a. REPORT SECURITY CLASSIFICATION
UNCLASSIFIED

2b. GROUP
N/A

3 REPORT TITLE
EXTERNAL FLOW-FIELD EFFECTS ON THE PLUME IMPINGEMENT PRESSURE AND HEAT-TRANSFER-RATE DISTRIBUTIONS ON A FLAT PLATE

4. DESCRIPTIVE NOTES *(Type of report and inclusive dates)*
Final Report - March 9 to 16, 1971

5. AUTHOR(S) *(First name, middle initial, last name)*
W. T. Strike, Jr. and D. E. Boylan, ARO, Inc.

6 REPORT DATE	7a. TOTAL NO. OF PAGES	7b. NO. OF REFS
September 1971	49	6

8a. CONTRACT OR GRANT NO.	9a. ORIGINATOR'S REPORT NUMBER(S)
F40600-72-C-0003	AEDC-TR-71-195
b. PROJECT NO.	
c. Program Element 65802F	9b. OTHER REPORT NO(S) *(Any other numbers that may be assigned this report)*
d.	ARO-VKF-TR-71-136

10. DISTRIBUTION STATEMENT
Approved for public release; distribution unlimited.

11. SUPPLEMENTARY NOTES	12. SPONSORING MILITARY ACTIVITY
Available in DDC	Arnold Engineering Development Center, Air Force Systems Command, Arnold AF Station, Tenn. 37389

13. ABSTRACT Experimental plume impingement pressure and heat-transfer-rate distributions on a flat plate with and without an external Mach number 18 stream are described. The plume was generated by expanding helium through a 1.61 area ratio nozzle, which simulated the initial shape of a rocket exhaust plume produced by a nozzle with an area ratio of 25 operating at an altitude of 262,000 ft. Although the plume generator nozzle conditions were not varied, the quiescent environment conditions and external stream conditions were adjusted so that the general shape and size of the plume remained the same. A higher quiescent pressure environment was required to produce a plume of the same size as the plume obtained in an external stream. In the immediate vicinity of the plume impingement on the flat plate within the plume boundary, the pressure distributions obtained with and without external flow were identical, but the overall change in surface loading produced by the plume was significantly affected by the external stream. The external stream also caused the local heat-transfer rates to increase significantly in the immediate vicinity of the plume boundary impingement point on the flat p plate. Therefore, any general assumption that aerodynamic external flowfield effects on plumes and on plume impingement loading and heat-transfer rates is negligible, even at an altitude of 262,000 ft, should be carefully examined.

DD FORM 1 NOV 65 1473

UNCLASSIFIED
Security Classification

14. KEY WORDS	LINK A		LINK B		LINK C	
	ROLE	WT	ROLE	WT	ROLE	WT
rocket exhaust						
missile plumes						
flow distribution						
booster rocket engines						
orbiter rocket engines						
test facilities						
flat plates						
heat transfer						
pressure distribution						
aerodynamic loads						

AFSC
Arnold AFS Tenn